TEST REPORT OF A 2.4GHZ IEEE 802.11b/g WLAN USB DONGLE, BRAND SAMSUNG, MODEL SWL-2610U, IN CONFORMITY WITH FEDERAL REGULATED SAR (SPECIFIC ABSORPTION RATE) REQUIREMENTS IN THE USA AND CANADA.

FCC listed	:	90828
Industry Canada	:	IC3501
VCCI registered	:	R-1518, C-1598

TNO Electronic Products & Services (EPS) B.V.
P.O. Box 15
9822 ZG Niekerk (NL)
Smidshornerweg 18
9822 TL Niekerk (NL)

Telephone: +31 594 505005
Telefax: +31 594 504804

E-mail: info@eps.tno.nl
Web: www.eps.tno.nl

Description of test item

Test item	:	2.4 GHz IEEE 802.11b/g WLAN USB Dongle
Manufacturer	:	SAMSUNG
Brand	:	SAMSUNG
Model	:	SWL-2610U
Serial numbers	:	MEJPKR-2270000239
Revision	:	n.a.
Receipt number	:	n.a.
Receipt date	:	June 17, 2004

Applicant information

Applicant's representative	:	M.Wouters van den Oudenweijer, B.Sc.
Company	:	Telefication B.V.
Address	:	Edisonstraat 12a
Postal code	:	6902 PK
City	:	Zevenaar
PO-box	:	n.a.
Postal code	:	n.a.
City	:	n.a.
Country	:	The Netherlands
Telephone number	:	+31 316 583 142
Telefax number	:	+31 316 583 189

Test(s) performed

Location	:	Niekerk
Test(s) started	:	June 18, 2004
Test(s) completed	:	June 18, 2004
Purpose of test(s)	:	To verify compliance with Federal regulated SAR requirements in the US and Canada
Test specification(s)		IEEE C95.1-1991, FCC OET Bulletin 65 (Supplement C), Industry Canada RSS-102 (Issue 1)
Test engineer	:	J. Schuurmans, B.Sc.E.E.
Report written by	:	J. Schuurmans, B.Sc.E.E.
Report approved by	:	P.A.J.M Robben
Report date	:	June 22, 2004

This report is in conformity with NEN-EN-ISO/IEC 17025: 2000.
This report shall not be reproduced, except in full, without the written permission of TNO Electronic Products & Services (EPS) B.V.
The test results relate only to the item(s) tested.

Table of contents

1 General. ... 5
1.1 Purpose of tests. ... 5
1.2 Applied standards/publications. ... 5
1.3 References. ... 5
2 Summary and conclusion. ... 6
2.1 Exposure category. ... 6
2.2 Summary of results. ... 6
2.3 Compliance. ... 6
3 Identification of Equipment Under Test (EUT). ... 7
3.1 Equipment under Test (EUT) details. ... 7
3.2 EUT test operating configurations. ... 7
3.3 Additional operating configurations. ... 8
4 Test conditions. ... 8
4.1 Environmental conditions. ... 8
4.2 System performance check 2.4 GHz. ... 8
4.2.1 2450 MHz validation parameters. ... 11
4.3 Measured maximum output power of EUT. ... 11
4.3.1 Measured Average power on 2.4 GHz. ... 11
4.4 Tissue simulating liquid dielectric parameters. ... 12
4.4.1 Mixing procedures. ... 12
4.4.2 Dielectric parameters for 2.4 GHz, body tissue. ... 13
4.4.3 Dielectric parameters for 2.4GHz, head tissue. ... 14
4.4.4 Tissue simulating liquid temperature requirements. ... 15
5 Photographs of EUT in host. ... 15
6 Identification of EUT-Phantom positions. ... 15
6.1 Portable Device operating near the body. ... 16
6.1.1 Position perpendicular. ... 16
6.1.2 Position lapheld. ... 17
7 Test Results. ... 18
7.1 Test methodology. ... 18
7.2 Results. ... 18
7.3 Step size and scan information. ... 18
8 Plots of measurement data. ... 19
8.1 Validation 2.4 GHz. ... 20
8.1.1 Host ACER, Lapheld channel 6. ... 21
8.1.2 Host ACER, Perpendicular channel 6. ... 22
8.2 Hotspot identification. ... 23

9 Description of test configuration. 24
9.1 SAR measurement system. 24
9.1.1 Robot System description. 24
9.1.2 Probe description. 24
9.1.3 Amplifier description. 25
9.1.4 Phantom description. 25
9.2 Measurement Procedure. 25
9.2.1 SARA2 Interpolation and Extrapolation schemes. 26
9.2.2 Interpolation of 2D area scan. 26
9.2.3 Extrapolation of 3D scan. 26
9.2.4 Interpolation of 3D scan and volume averaging. 26
10 Additional information supplementary to the test report. 28
10.1 Probe information. 28
10.2 SAR system check. 28
10.3 5.8 GHz system check. 29
10.3.1 Introduction. 29
10.3.2 Validation results using WR187 waveguide. 30
10.3.3 An alternative open-ended waveguide geometry. 30
10.4 Dielectric property measurement of tissue-simulant liquids for SAR testing. 32
10.4.1 Introduction. 32
10.4.2 TEM-cell construction. 32
10.4.3 Calculation of dielectric properties from VNA measurements. 32
10.5 Measurement uncertainty. 33
10.5.1 Introduction. 33
10.5.2 Uncertainty calculated for IEEE1528 : standard measurements (2450 MHz). 34
10.5.3 Uncertainty calculated for IEEE1528 : standard measurements (5800 MHz). 35
10.5.4 Uncertainty calculated for IEEE1528 : System performance check (2450 MHz). 36
10.5.5 Uncertainty calculated for IEEE1528 : System performance check (5800 MHz). 37
11 List of utilized test equipment. 38
12 Test software. 38

Annexes:

- Calibration Certificate Dosimetric E-field Probe.
- Immersible SAR probe calibration report IXP – 050 S/N 0131
- IndexSAR report no. IXS-0223, Compensating for the finite size of SAR probes used in electric field gradients

1 General.

1.1 Purpose of tests.

Tests were conducted to verify compliance with Federal regulated SAR requirements in the US and Canada.

1.2 Applied standards/publications.

The Equipment Under Test (EUT) was tested in conformity with the described test method(s) in the following Standards and/or publications:

- IEEE Std C95.1-1999 edition: IEEE Standard for Safety Levels with Respect to Human Exposure to Radio Frequency Electromagnetic Fields, 3kHz to 300GHz

- FCC OET Bulletin 65 (Supplement C) edition 01-01: Evaluating Compliance with FCC Guidelines for Human Exposure to radio Frequency Fields. Additional information for evaluating Compliance of Mobile and Portable Devices with FCC limits for Human Exposure to Radiofrequency Emissions.

- Industry Canada RSS-102 (Issue 1).

1.3 References.

The methods and procedures applicable to measurements as performed and indicated in this test report are also described in detail in the following reference documents:

Publications	Year	Title
IEEE Std. 1528	2003	Recommended Practice for Determining the Peak Spatial-Average Specific Absorption rate (SAR) in the Human Head from Wireless Communications Devices: Measurement Techniques.
FCC OET Bulletin 65, Edition 97-01	1997	Evaluating Compliance with FCC Guidelines for Human Exposure to radio Frequency Fields
ANSI/IEEE C95.3	2002	IEEE Recommended Practice for the Measurement and Computations of Radio Frequency Electromagnetic Fields With Respect to Human Exposure to Such Fields, 100kHz-300GHz

2 Summary and conclusion.

2.1 Exposure category.

The EUT is a portable device used near the body.
According to the characteristics of the EUT and typical application and usage in accordance with the relevant product specifications of the manufacturer the EUT is identified to the exposure category:

General population/Uncontrolled exposure.

2.2 Summary of results.

In the 2.4 GHz frequency range (2412 – 2477 MHz) the maximum peak spatial-average SAR measured was 0.153 W/Kg averaged over 1g with the EUT transmitting on 2437 MHz (channel 6) at a power level of 19 dBm (conducted average including 3 dBi antenna gain) while the EUT was positioned in lapheld fashion.

2.3 Compliance.

The equipment was found to be compliant with requirements of standards as indicated in the table below:

Exposure Category and SAR Limits	Test Requirements	Compliance (Yes/No)
Limit value for as per 47 CFR Ch 1.1093 (d)(2): spatial peak SAR shall not exceed **1.6 W/kg** as averaged over 1 g of tissue.	Requirements using guidelines established in:	
	IEEE C95.1-1991	Yes/~~no~~
	FCC OET Bulletin 65 (Supplement C)	Yes/~~no~~
	Industry Canada RSS-102 (Issue 1).	Yes/~~no~~

3 Identification of Equipment Under Test (EUT).

The following is the information provided by the applicant.

3.1 Equipment under Test (EUT) details.

Description	Model number	Serial number	FCC ID	Cable descriptions
2.4 GHz IEEE 802.11b/g WLAN USB dongle	SWL-2610U	MEJPKR-2270000239	E2XSWL-2610U	None.
laptop Acer	Travelmate 350 2001	9145H018S510800AC0M	DoC	
AC Adpater Acer 19V 3.2A	PA-1600-02	1229852CA	DoC	Supply cable / AC power cord

3.2 EUT test operating configurations.

Modulation type/ operating modes	:	DSSS (1, 2, 5.5, 11 MBit/s), OFDM (6, 9, 11, 54 MBit/s), BPSK, QPSK, 16QAM, 64 QAM
Operating frequency range	:	2400-2483.5 MHz (11 channels)
Maximum indicated power	:	16 dBm average power incl antenna gain @ 2412 MHz – 2472 MHz
Duty cycle during testing	:	100%
Antenna type(s) and gain	:	Integral, gain 0 dBi @ 2.4 GHz.
Power supply/ power source	:	See section 3.1
Primary User Functions of EUT	:	Data Radio Communication through Air
EUT Accessories	:	See section 3.1
Hardware/software changes applied for testing	:	EUT is made to transmit with 100% duty cycle, by means of specific test software supplied by applicant.

3.3 Additional operating configurations.

Power and signal distribution, grounding, interconnecting cabling and physical placement of the EUT under circumstances of testing at the test system are in accordance with the typical application and usage in so far as is practicable, and is in accordance with the relevant product specifications of the manufacturer.

The configuration of the EUT and its position are fully detailed and documented in the test report.

4 Test conditions.

4.1 Environmental conditions.

Requirement for	Specification	Determined value
Ambient temperature	+18°C to +25°C Temperature shall not exceed ±2 °C during the test	+21°C to +23°C
Ambient humidity	20% to 75%	45%-55%
Electro Magnetic environment	the ambient interference power shall be less than 0,012 W/kg	below the required lower detection limit of 0,010 W/kg, checked before and after test

4.2 System performance check 2.4 GHz.

The purpose of the system performance check (*system check*) is to verify that the system operates within its specifications at the device test frequency. The system check is to make sure that the system works correctly at the time of the compliance test. The system check has been performed using the specified tissue-equivalent liquid and at a chosen fixed frequency that is within ± 10% of the compliance test mid-band frequency. The system check is performed prior to compliance tests and the result must always be within ±10% of the target value corresponding to the test frequency, liquid and the source used. In section 10.3 a description of this check is given. Below photographs of the 2.4 check instrument setup and validation dipoles.

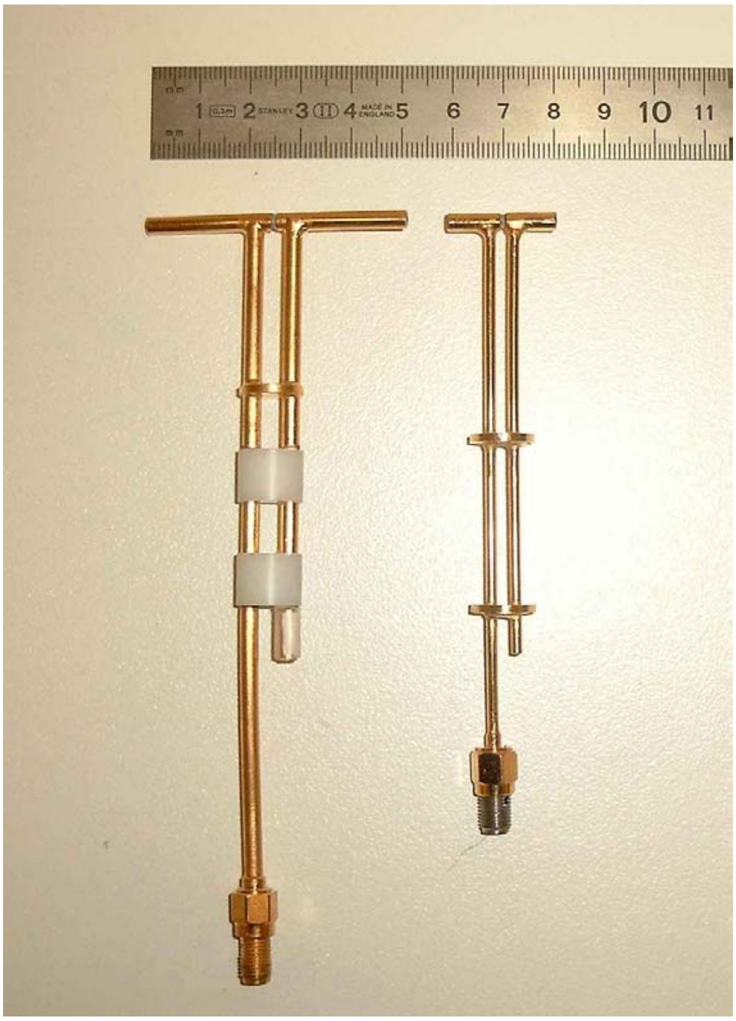

Photo 1: validation dipoles

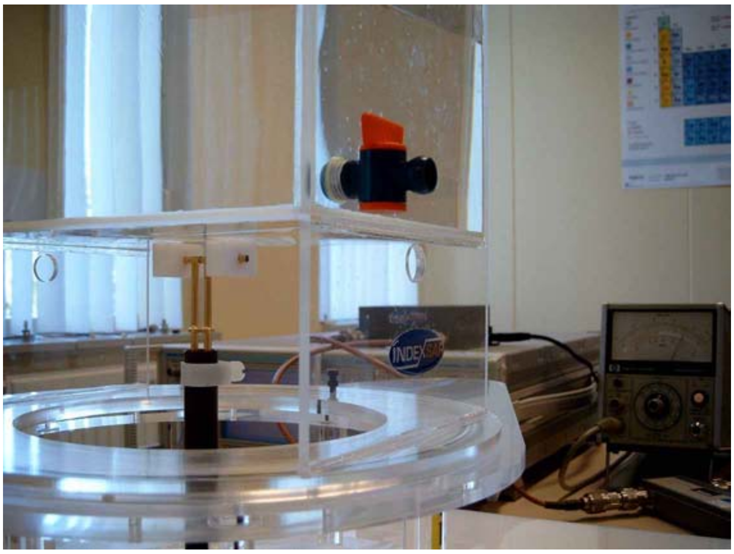

Photo 2: 2.4 GHz dipole validation

Photo 3: instrument setup system check

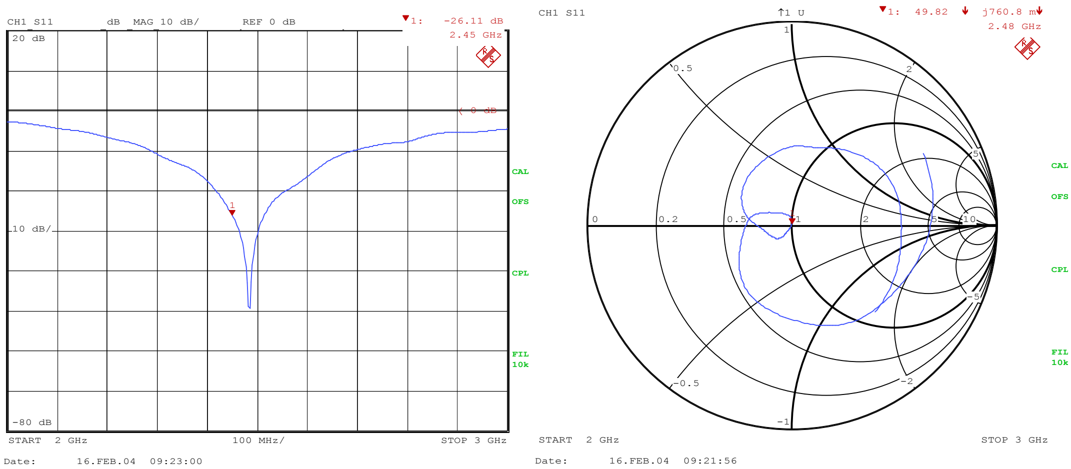

Figure 1: |S11| and S11 smith chart of the 2.4 GHz dipole placed underneath the filled phantom

The target values are 1 g or 10 g averaged SAR values measured on systems for which s*ystem validation* has been performed.

4.2.1 2450 MHz validation parameters.

The following system performance check results were obtained in accordance with Chapter 8 of IEEE 1528 of December, 2003:

At 2450 MHz a system validation was executed according IEEE Std. 1528-2003 . Dipole used see Photo 1.

Frequency = 2477 MHz	Target value	Measured value	Deviation[1]
Peak Spatial-Average SAR 1g [W/kg]	52	51.76	-0.4 %
Peak Spatial-Average SAR 10g [W/kg]	24	26.12	+8.3%

Detailed validation results may be found in section 8.

4.3 Measured maximum output power of EUT.

The EUT has been set to the maximum output power level that is defined by the manufacturer and/or the operating requirements of the system (see section 3.3 EUT test operating configurations).

The results of tests on the EUT are depicted in table below. Listed is the higher of the conducted average power and EIRP.

4.3.1 Measured Average power on 2.4 GHz.

Transmission bit rate DSSS mode (Mbit/s)	Average transmit output power (conducted, dBm)		
	Channel 1 (2412 MHz)	Channel 6 (2437 MHz)	Channel 11 (2462 MHz)
1	15.4	15.9	15.9
2	15.4	15.9	15.9
5.5	15.4	15.9	15.9
11	15.4	15.9	15.9

Table 1: Average output power including antenna gain

Transmission bit rate OFDM mode (Mbit/s)	Average transmit output power (conducted, dBm)		
	Channel 1 (2412 MHz)	Channel 6 (2437 MHz)	Channel 11 (2462 MHz)
6	16.0	16.0	16.0
18	14.2	14.4	14.4
36	12.1	12.1	12.4
54	10.1	10.4	10.4

Table 2: Average output power including antenna gain

[1] Deviation is calulated: 100% *((measured value)/(reference value) –1)

From table 1 and 2 it can be seen that in channel 6 the highest power is found. First SAR scan will therefore be performed at channel 6, using OFDM 6 Mb/s (See also section 7.1).

Transmission bit rate (Mbit/s)	Average transmit output power drift [dB]
	Channel 6 (2437 MHz)
OFDM 9	Less than 0.2 dB

Table 3: average output power drift

4.4 Tissue simulating liquid dielectric parameters.

For the purpose of the tests as described in this report the following tissue dielectric parameters have been determined
The tables indicate the dielectric parameters of the liquids used during the tests. The indicated required values are derived from IEEE Std. 1528-2003 and OET Bulletin 65 supplement C. At frequencies other than reference frequencies, for which tissue parameters are given in the standards, the parameters have been determined by the linear interpolation. Depending the intended use of the EUT the interpolated values will refer to the mid-band frequency of each operating mode.
The measurement method is described in section 10.4.

Deviation of the actual parameters vs. the prescribed parameters is calculated according: D=(A/T –1)*100% where D is deviation in %, A is the actual value and T is the Target value.

4.4.1 Mixing procedures.

All Tissue Equivalent Liquids are obtained from Bristol University.
Contact details:
Medical Physics Department
University of Bristol, Bristol Haemotology & Oncology Centre
Horfield road, Bristol BS2 8 ED, United Kingdom
Tel. 44 117 928 2469.

4.4.2 Dielectric parameters for 2.4 GHz, body tissue.

MHz	εr [ε']	σ [S/m]	εr [ε'] Min	εr [ε'] Max	σ [S/m] Min	σ [S/m] Max	Measured εr [ε']	Measured Δ(%)	Measured σ [S/m]	Measured Δ(%)
2412	52.75	1.91	47.78	58.03	1.72	2.11	52.72	-0.05%	1.96	2.57%
2437	52.72	1.94	47.45	57.99	1.74	2.13	52.67	-0.10%	1.99	2.48%
2462	52.679	1.97	47.42	57.95	1.77	2.16	52.57	-0.20%	2.02	2.46%

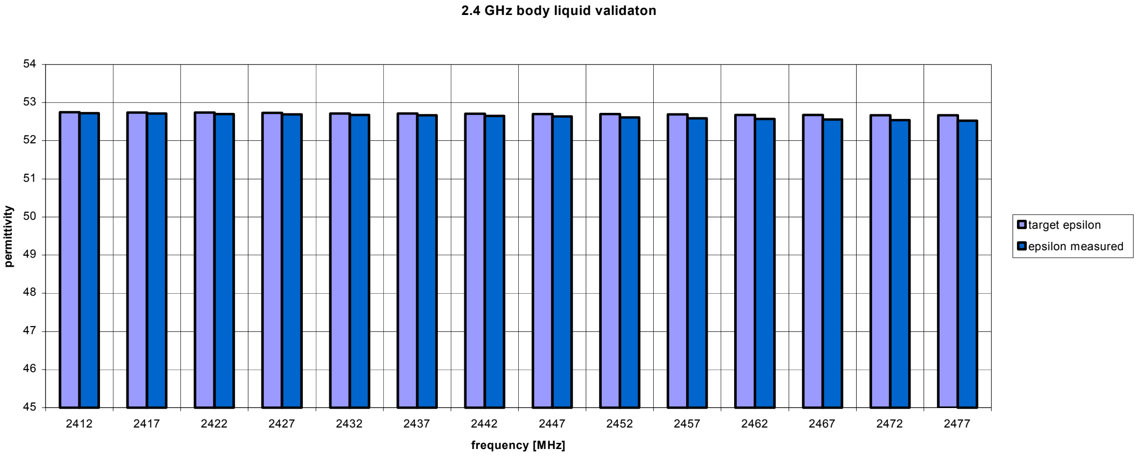

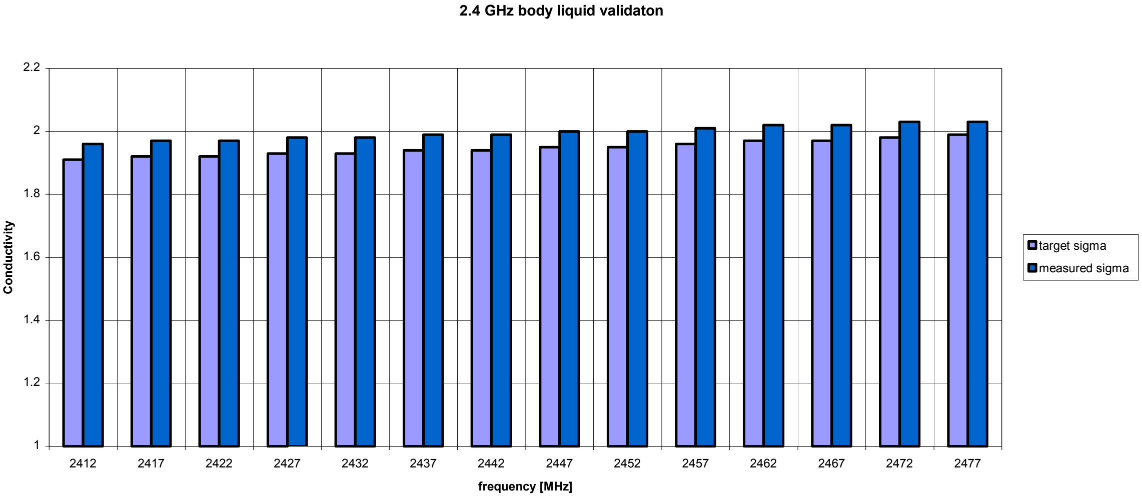

4.4.3 Dielectric parameters for 2.4GHz, head tissue.

MHz	εr [ε']	σ [S/m]	εr [ε']		σ [S/m]		Measured			
			Min	Max	Min	Max	εr [ε']	Δ(%)	σ [S/m]	Δ(%)
2412	39.27	1.77	47.78	58.03	1.72	2.11	39.97	1.78%	1.67	-5.44%
2437	39.22	1.79	47.45	57.99	1.74	2.13	39.92	1.77%	1.71	-4.27%
2462	39.18	1.81	47.42	57.95	1.77	2.16	39.83	1.67%	1.75	-3.42%

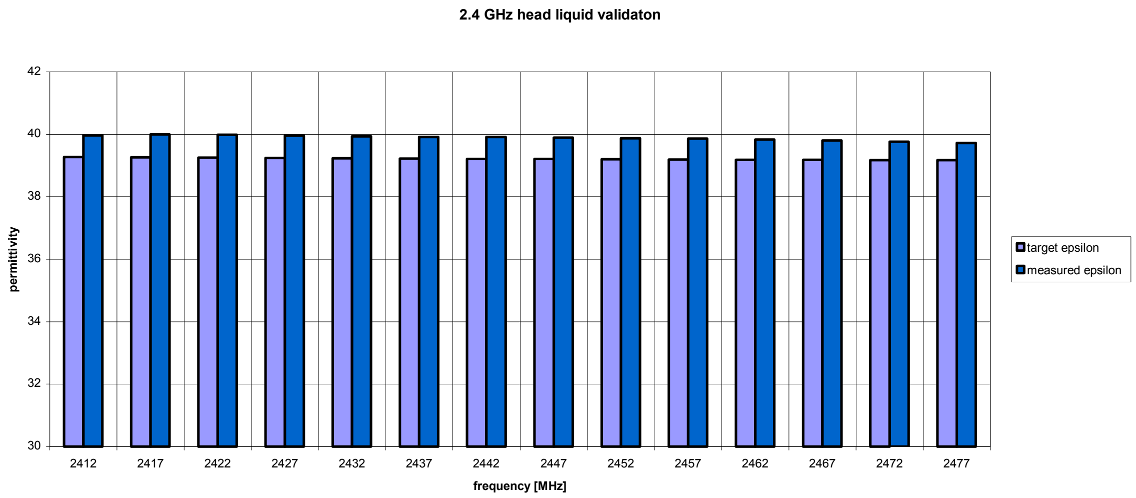

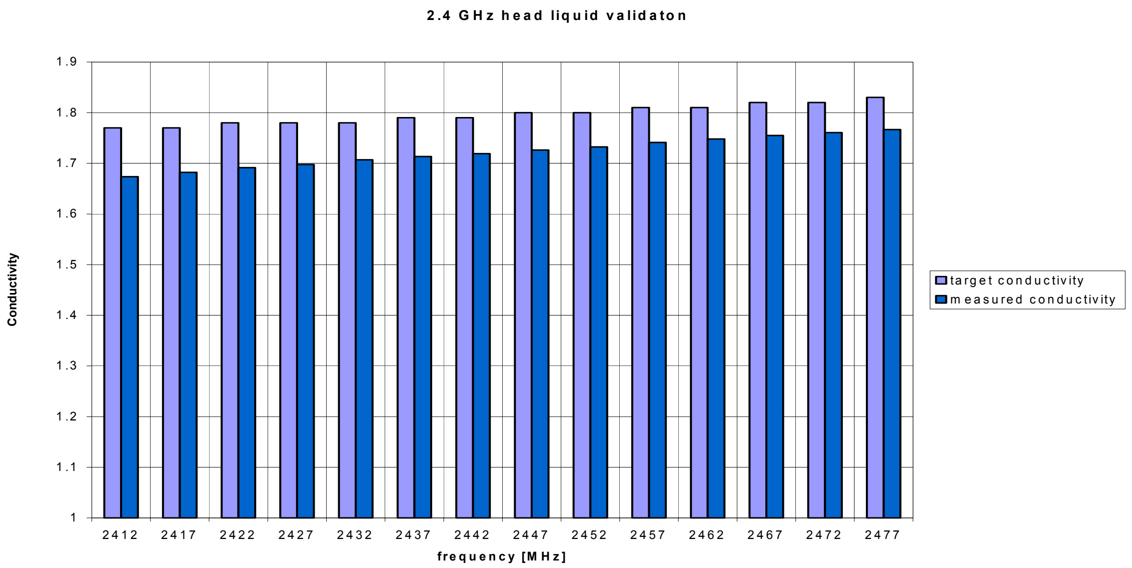

4.4.4 Tissue simulating liquid temperature requirements.

The variation of the liquid temperature shall not exceed ±2° C during the test; The actual tissue simulating liquid temperature was recorded to be between 22.0° C to 22.5° C).

5 Photographs of EUT in host.

Photo 4 Front view with dongle inserted.

Photo 5 : Side view. Offset dongle to base = 8 mm

6 Identification of EUT-Phantom positions.

6.1 Portable Device operating near the body.

Following the guidelines from FCC OET bulletin 65 C and the TCB RF exposure training notes, 2 positions were investigated. The 'lapheld' position reflects the situation where the laptop is placed on the users lap. The laptop containing the EUT is placed underneath the flat phantom with the EUT placed in the bottom slot, thus minimizing the distance of the EUT and the users body.

The second position reflects bystander SAR. This position means that the card is facing the phantom bottom shell perpendicularly. The position is referred to as 'perpendicular'. The separation distance is 10 mm, which still yields a useful reading of the field strength in the liquid.

6.1.1 Position perpendicular.

The separation distance, *d* of 10 mm measured from side of the EUT to the bottom of the phantom.

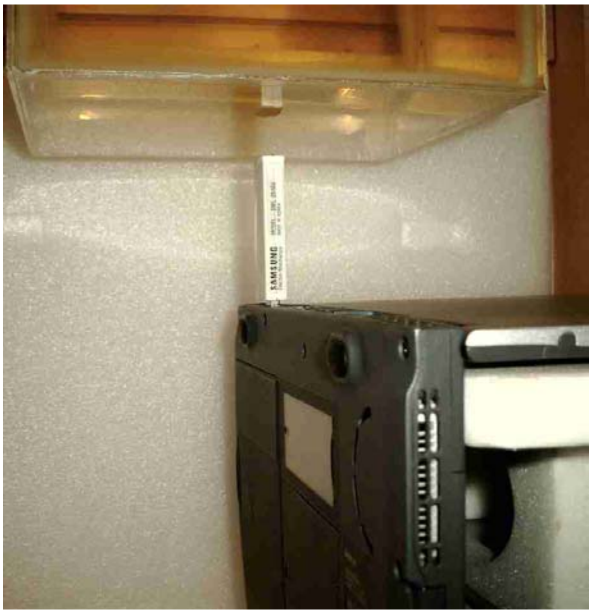

Photo 6 Perpendicular

6.1.2 Position lapheld.

This position follows the directions from FCC TCB training notes dated April 2002. This position reflects the situation where the user had the laptop on his or her lap, with the card inserted in the lower slot.
The separation distance, *d* was determined to be 13 mm, and reflects the position where the host would be positioned on the lap.

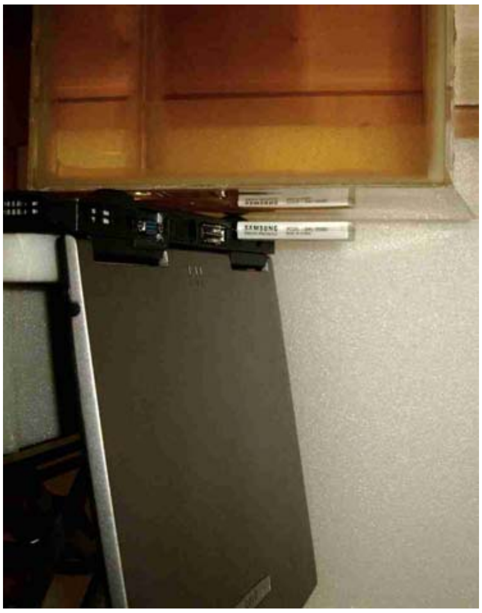

Photo 7 Position lapheld

7 Test Results.

7.1 Test methodology.

SAR evaluation starts with determining at which channels/modulation/bitrate combination SAR scans have to be performed. To do this, average conducted power is measured for all modulations and bitrates. From these measurements, in a given channel the modulation/bitrate is found by looking at the highest power found in that channel. In that channel, SAR is measured at that bitrate and modulation type. Should it appear that SAR tests in that channel show higher SAR than half the limit, SAR is also measured in the highest and lowest channel is that band. After testing, the channel with highest SAR found is rechecked by measureing Spot SAR in that channel while setting all modulation and bitrates. Should a higher value be found, a full SAR scan is performed for that particular bitrate/modulation. The highest value found is be reported.

7.2 Results.

Host	Distance base to bottom USB dongle	Channel / modulation	Lapheld contact PSA[2] SAR 1g (W/kg)	Perpendicular + 5 mm PSA SAR (1g) (W/kg)
ACER	8 mm	1 (2412) OFDM 6 Mbit/s	n.a.	n.a.
		6 (2437) OFDM 6 MBit/s	0.153	0.039
		11 (2462) OFDM 6 MBit/s	n.a.	n.a.

Note: n.a. means that SAR measured in the channel with highest power is lower than 3 dB below the SAR limit, testing of the indicated channels is optional [ref: OET bull 65 suppl C p. 40). The channels n.a. have not been measured.

7.3 Step size and scan information.

Measurements on 2.4 GHz: A 35x35 mm area is scanned centered around the hotspot using 7 steps in the x-y plane and 10 steps of 3.5 mm in the z plane. The first area scan is performed with the probe tip 5 mm above the phantom bottom shell

The location of the hotspot is determined prior to each 3D scan by means of an area scan.

[2] PSA SAR is Peak Spatial-Average SAR.

8 Plots of measurement data.

section	Ch	EUT position
01	-	Validation 2.4 GHz
02	6	Lapheld
03	6	Perpendicular 10mm

8.1 Validation 2.4 GHz.

Device Under Test:		**Validation dipole**	
HOST		**n.a.**	
Position / Channel		**n.a.**	
DATE [dd/mm/yyyy]		**17-06-2004**	
System / software:		SARA v2.3	
Phantom S/No:	Box phantom.	No. of steps x and y	7
Test Frequency [MHz]	2447	Stepsize x and y [mm]	5
Antenna Configuration:	Dipole	No of steps z	10
Power / (setting(s) [dBm]	24	Stepsize z [mm]	3.5
Type of Modulation:	CW	Dist probe tip – phantom shell [mm]	5
Modn. Duty Cycle [%]	100	Prove conversion factor …..	0.534
Probe Serial Number:	131	Probe battery check [d/m/y]:	17-06-2004
Liquid Simulant:	Head	Max E-field [V/m in liquid]	72.24
Permittivity / Conductivity [S/m]	39.2 / 1.8	Location of max. X= [mm]	3.5
Liquid Temperature [C]	22.0	Location of max Y= [mm]	0.5
Ambient Temperature [C]	23.0	Location of max Z= [mm]	-211.5
Relative Humidity [%]	52	SAR Drift: [dB]	0
Results:			
SAR 1g [W/kg]:	12.94		
SAR 10g [W/kg]:	6.53		

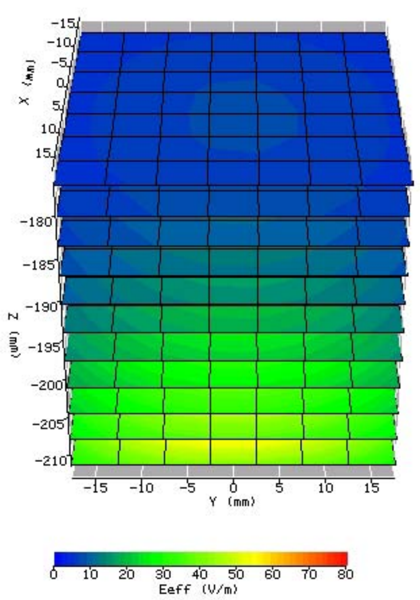

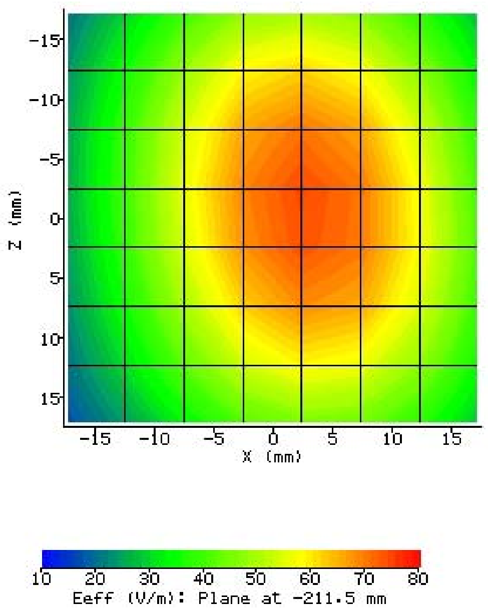

8.1.1 Host ACER, Lapheld channel 6.

Device Under Test:		**SAMSUNG SWL-2610U WLAN USB dongle**	
HOST		**ACER**	
Position / Channel		**lapheld**	
DATE [dd/mm/yyyy]		**17-06-2004**	
System / software:		SARA v2.3	
Phantom S/No:	Box phantom.	No. of steps x and y	7
Test Frequency [MHz]	2437	Stepsize x and y [mm]	5
Antenna Configuration:	Integral	No. of steps z	10
Power / (setting(s) [dBm]	19	Stepsize z [mm]	3.5
Type of Modulation, datarate [Mb/s]:	OFDM, 6	Dist probe tip – phantom shell [mm]	5
Modn. Duty Cycle [%]	100	Prove conversion factor …..	0.540
Probe Serial Number:	131	Probe battery check [dd/mm/yyyy]:	17-06-2004
Liquid Simulant:	Body	Max E-field [V/m in liquid]	7.62
Permittivity / Conductivity [S/m]	52.7 / 1.94	Location of max. X= [mm]	-2.75
Liquid Temperature [C]	22.0	Location of max Y= [mm]	6.25
Ambient Temperature [C]	23.0	Location of max Z= [mm]	-474.5
Relative Humidity [%]	50.0	SAR Drift: [dB]	0.5
Results:			
SAR 1g [W/kg]:	0.153		
SAR 10g [W/kg]:	0.086		

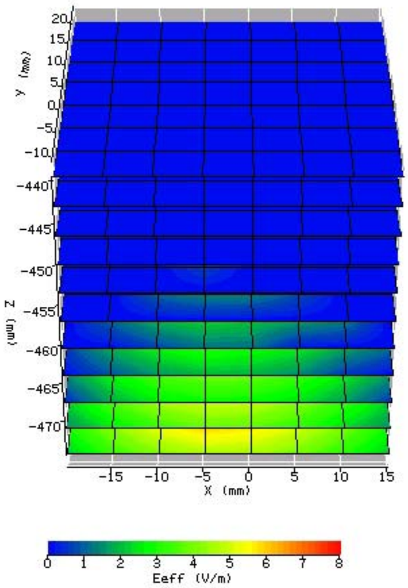

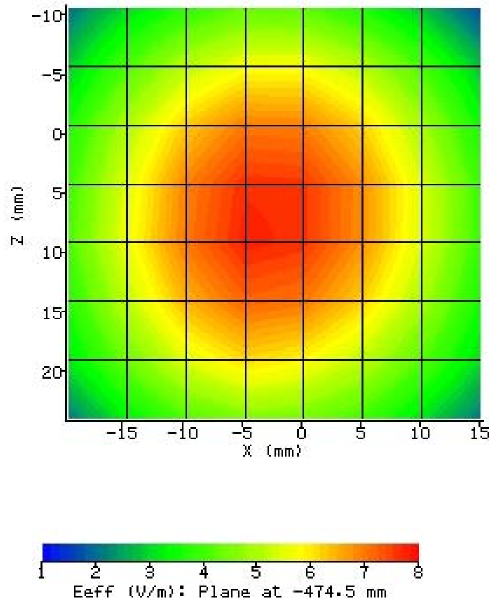

8.1.2 Host ACER, Perpendicular channel 6.

Device Under Test:		**SAMSUNG SWL-2610U WLAN USB dongle**	
HOST		**ACER**	
Position / Channel		**lapheld**	
DATE [dd/mm/yyyy]		**17-06-2004**	
System / software:		SARA v2.3	
Phantom S/No:	Box phantom.	No. of steps x and y	7
Test Frequency [MHz]	2437	Stepsize x and y [mm]	5
Antenna Configuration:	Integral	No. of steps z	10
Power / (setting(s) [dBm]	19	Stepsize z [mm]	3.5
Type of Modulation, datarate [Mb/s]:	OFDM, 6	Dist probe tip – phantom shell [mm]	5
Modn. Duty Cycle [%]	100	Prove conversion factor …..	0.540
Probe Serial Number:	131	Probe battery check [dd/mm/yyyy]:	17-06-2004
Liquid Simulant:	Body	Max E-field [V/m in liquid]	3.53
Permittivity / Conductivity [S/m]	52.7 / 1.94	Location of max. X= [mm]	-2.75
Liquid Temperature [C]	22.5	Location of max Y= [mm]	9.75
Ambient Temperature [C]	23.0	Location of max Z= [mm]	-474.5
Relative Humidity [%]	50.0	SAR Drift: [dB]	n.a.
Results:			
SAR 1g [W/kg]:	0.039		
SAR 10g [W/kg]:	0.025		

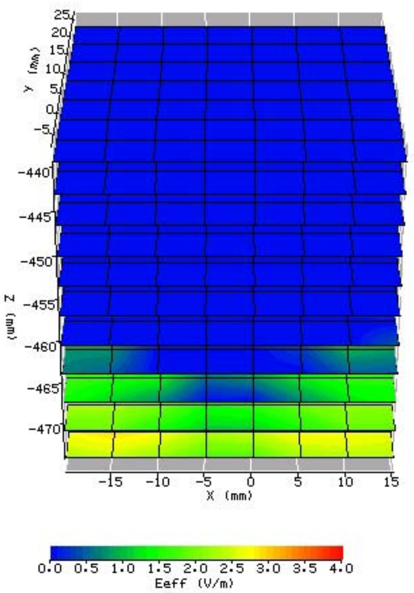

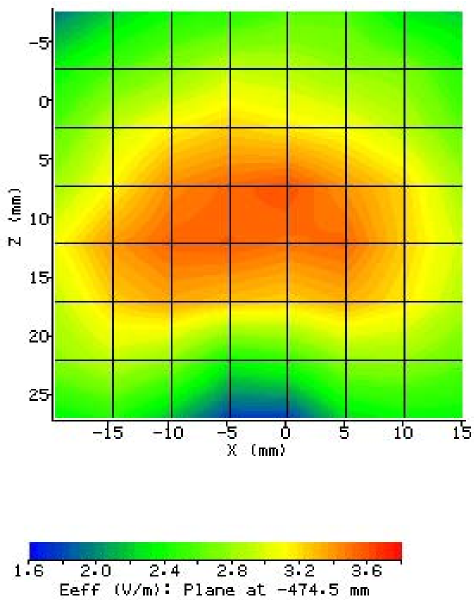

8.2 Hotspot identification[3]

By means of an overlay of the 2d scan and a EUT photograph the location and orientation of the hotspot is given.

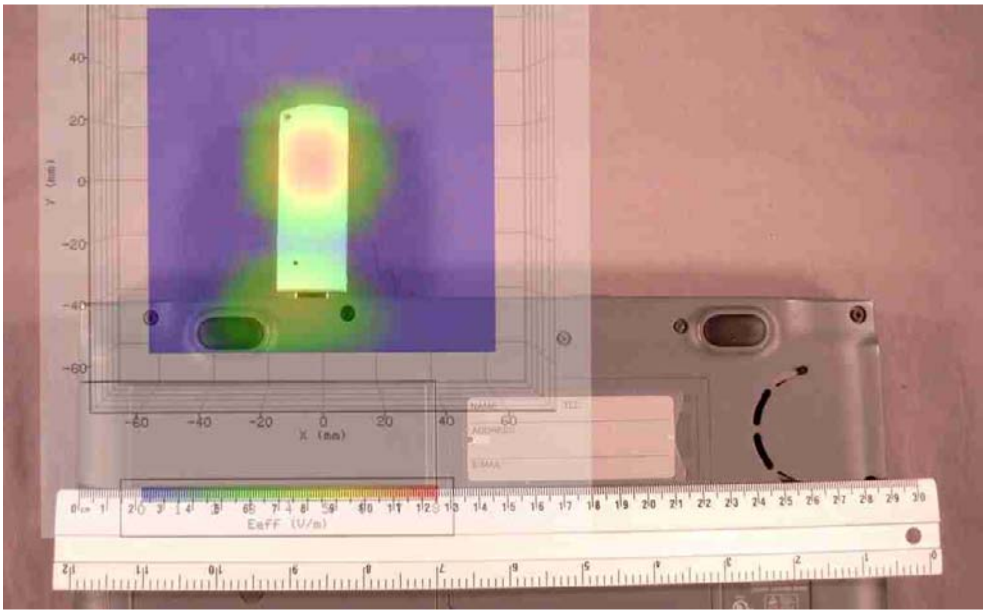

Photo 6: A 2d scan overlay giving the field strength in the first sanned plane, overlaid on a bottom side view photo of the laptop. 2d scan is that of the worst case lapheld value in channel 6.

[3] The hotspot is indicated with approximate values.

9 Description of test configuration.

9.1 SAR measurement system.

9.1.1 Robot System description.

The SAR measurement system used by TNO EPS is the IndexSAR SARA2 system, which consists of a Mitsubishi RV-2A six-axis robot-arm and controller, IndexSAR probe and amplifier and an appropriate phantom as required and considered appropriate for the applied test. The robot is used to move and manipulate the probe to programmed positions inside the phantom to obtain the SAR readings from the EUT.

The system is remote controlled by a PC, which contains the software to control the robot and data acquisition equipment. The software also displays the data obtained from test scans by calculating the measured values into corresponding SAR values based on the currently acceptable calculation methods.

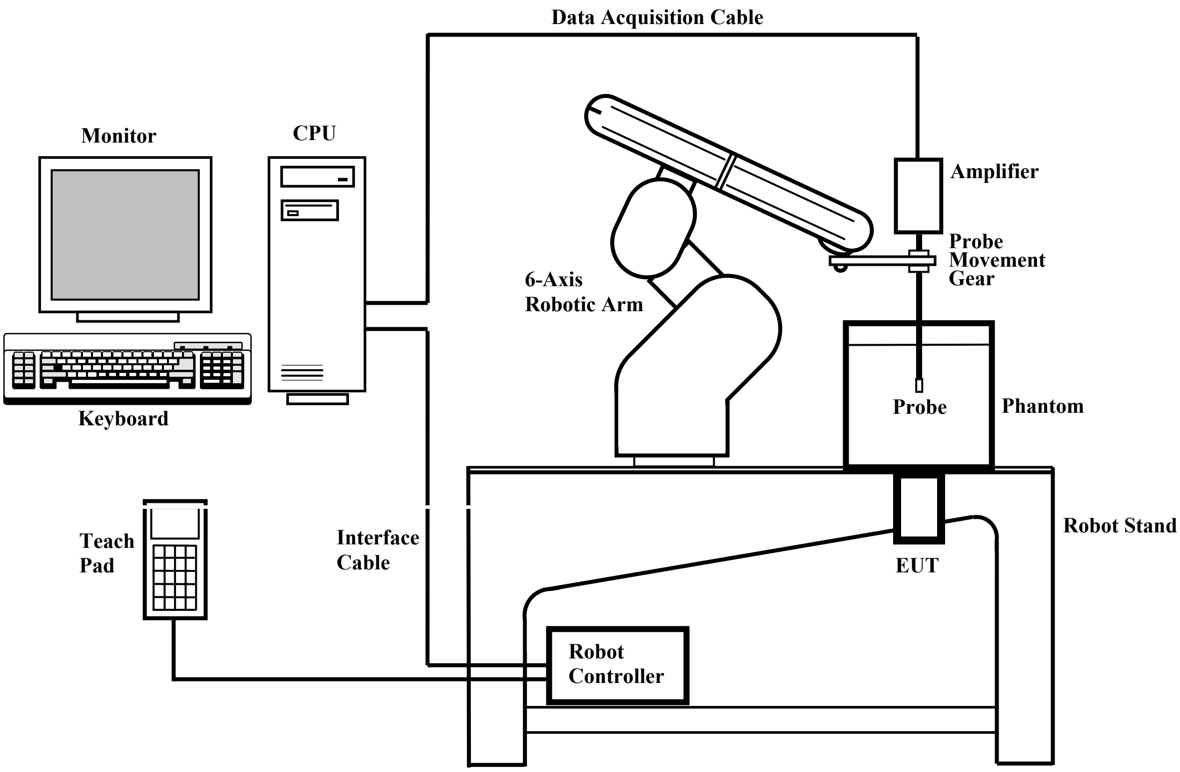

Figure 1: Overview of the SARA2 measurement system

The position and digitized shape of the phantom are made available to the software for accurate positioning of the probe and reduction of set-up time.

E.g. the SAM phantom heads are individually digitized using a Mitutoyo CMM machine to a precision of 0.001mm. The data is then converted into a shape format for the software, providing an accurate description of the phantom shell.

In operation, the system first does an area (2D) scan at a fixed depth within the liquid from the inside wall of the phantom. When the maximum SAR point has been found, the system will then carry out a 3D scan centered at that point to determine volume averaged SAR level.

9.1.2 Probe description.

The probes are constructed using three orthogonal dipole sensors arranged on an interlocking, triangular prism core. The probes have built-in shielding against static charges and are contained within a PEEK cylindrical enclosure material at the tip.

Probe calibration is described in section 10.1.

9.1.3 Amplifier description.

The amplifier unit has a multi-pole connector to connect to the probe and a multiplexer selects between the 3-channel single-ended inputs. A 16-bit AtoD converter with programmable gain is used along with an on-board micro-controller with non-volatile firmware. Battery life is around 150 hours and data are transferred to the PC via 3m of duplex optical fibre and a self-powered RS232 to optical converter.

9.1.4 Phantom description.

Body-worn operating configurations are tested using a flat phantom. The body phantom shell is made of a low-loss dielectric material with dielectric constant and loss tangent less than 5.0 and 0.05 respectively. The shell thickness for all regions coupled to the test device and its antenna are within 2.0 ± 0.2 mm. The phantom was filled with the required head or body equivalent tissue medium to a depth of 15.0 ± 0.5 cm.

For body mounted and frontal held push-to-talk devices, a flat phantom of dimensions 20x20x20cm with a base plate thickness of 2mm is used.

For Head mounted devices placed next to the ear, the phantom used in the evaluation of the RF exposure of the user of the wireless device is a IEEE P1528/CENELEC EN50361 compliant phantom, shaped like a human head and filled with a mixture simulating the dielectric characteristics of the brain.

The for SARA2 measurement system used Specific Anthropomorphic Mannequin (SAM) Upright Phantom is fabricated using moulds generated from the CAD files as specified by CENELEC EN50361. It is mounted via a rotation base to a supporting table, which also holds the robotic positioner. The phantom and robot alignment is assured by both mechanical and laser registration systems.

9.2 Measurement Procedure.

During the SAR measurement, the positioning of the probe is performed with sufficient accuracy to obtain repeatable measurements in the presence of rapid spatial attenuation phenomena. The accurate positioning of the E-field probe is accomplished by using the high precision robot. The robot can be taught to position the probe sensor following a specific pattern of points.

After an area scan has been done at a fixed distance of 8mm from the side of the phantom on the source side, a 3D scan is set up around the location of the maximum spot SAR. First, a point within the scan area is visited by the probe and a SAR reading taken at the start of testing. At the end of testing, the probe is returned to the same point and a second reading is taken. Comparison between these start and end readings enables the power (SAR) drift during measurement to be assessed.

9.2.1 SARA2 Interpolation and Extrapolation schemes.

SARA2 software contains support for both 2D cubic B-spline interpolation as well as 3D cubic B-spline interpolation. In addition, for extrapolation purposes, a general n^{-th} order polynomial fitting routine is implemented following a singular value decomposition algorithm presented in [4]. A 4^{th} order polynomial fit is used by default for data extrapolation, but a linear-logarithmic fitting function can be selected as an option. The polynomial fitting procedures have been tested by comparing the fitting coefficients generated by the SARA2 procedures with those obtained using the polynomial fit functions of Microsoft Excel when applied to the same test input data.

9.2.2 Interpolation of 2D area scan.

The 2D cubic B-spline interpolation is used after the initial area scan at fixed distance from the phantom shell wall. The initial scan data are collected with approx. 10mm spatial resolution and spline interpolation is used to find the location of the local maximum to within a 1mm resolution for positioning the subsequent 3D scanning.

9.2.3 Extrapolation of 3D scan.

For the 3D scan, data are collected on a spatially regular 3D grid having (by default) 6.4 mm steps in the lateral dimensions and 3.5 mm steps in the depth direction (away from the source). SARA2 enables full control over the selection of alternative step sizes in all directions. The digitized shape of the Flat Phantom is available to the SARA2 software, which decides which points in the 3D array are sufficiently well within the shell wall to be ‘visited’ by the SAR probe. After the data collection, the data are extrapolated in the depth direction to assign values to points in the 3D array closer to the shell wall. A notional extrapolation value is also assigned to the first point outside the shell wall so that subsequent interpolation schemes will be applicable right up to the shell wall boundary.

9.2.4 Interpolation of 3D scan and volume averaging.

The procedure used for defining the shape of the volumes used for SAR averaging in the SARA2 software follow the method of adapting the surface of the ‘cube’ to conform with the surface of the phantom (see Appendix C.2.2.1 in EN 50361). This is called, here, the conformal scheme.

For each row of data in the depth direction, the data are extrapolated and interpolated to less than 1mm spacing and average values are calculated from the phantom surface for the row of data over distances corresponding to the requisite depth for 10g and 1g cubes. This results in two 2D arrays of data, which are then cubic B-spline interpolated to sub mm lateral resolution. A search routine then moves an averaging square around through the 2D array and records the maximum value of the corresponding 1g and 10g volume averages. For the definition of the surface in this procedure, the digitized position of the headshell surface is used for measurement in head-shaped phantoms. For measurements in rectangular, box phantoms, the distance between the phantom wall and the closest set of gridded data points is entered into the software.

For measurements in box-shaped phantoms, this distance is under the control of the user. The effective distance must be greater than 2.5mm as this is the tip-sensor distance and to avoid interface proximity effects, it should be at least 5mm. A value of 6 or 8mm is recommended. This distance is called **dbe** in EN 50361.

For automated measurements inside the head, the distance cannot be less than 2.5mm, which is the radius of the probe tip and to avoid interface proximity effects, a minimum clearance distance of x mm is retained. The actual value of dbe will vary from point to point depending upon how the spatially-regular 3D grid points fit within the shell. The greatest separation is when a grid point is just not visited due to the probe tip dimensions. In this case the distance could be as large as the step-size plus the minimum clearance distance (i.e with x=5 and a step size of 3.5, **dbe** will be between 3.5 and 8.5mm).

The default step size (**dstep** in EN 50361) used is 3.5mm, but this is under user-control. The compromise is with time of scan, so it is not practical to make it much smaller or scan times become long and power-drop influences become larger.

The robot positioning system specification for the repeatability of the positioning (**dss** in EN50361) is +/- 0.04mm.

The Specific Anthropomorphic Mannequin (SAM) Upright Phantom shell is made by an industrial moulding process from the CAD files of the SAM shape, with both internal and external moulds. For the upright phantoms, the external shape is subsequently digitized on a Mitutoyo CMM machine (Euro C574) to a precision of 0.001mm. Wall thickness measurements made non-destructively with an ultrasonic sensor indicate that the shell thickness (**dph**) away from the ear is 2.0 +/- 0.1mm. The ultrasonic measurements were calibrated using additional mechanical measurements on available cut surfaces of the phantom shells.

The flat phantom is made from Polymethylmethacrylate (PMMA), a low-loss dielectric material with dielectric constant and loss tangent less than 5.0 and 0.05 respectively. The shell thickness for all regions coupled to the test device and its antenna are within 2.0 ± 0.2 mm.

For the upright phantom, the alignment is based upon registration of the rotation axis of the phantom on its 253mm-diameter baseplate bearing and the position of the probe axis when commanded to go to the axial position. A laser alignment tool is provided (procedure detailed elsewhere). This enables the registration of the phantom tip (**dmis**) to be assured to within approx. 0.2mm. This alignment is done with reference to the actual probe tip after installation and probe alignment. The rotational positioning of the phantom is variable – offering advantages for special studies, but locating pins ensure accurate repositioning at the principal positions (LH and RH ears).

10 Additional information supplementary to the test report.

10.1 Probe information.

To this report the probe test report and calibration document of the probe used are added. In the electronic version of this report, the pages are inserted after the last page of this report.

10.2 SAR system check.

The purpose of the SAR System check is to verify that the system operates within its specifications at the device test frequency. The SAR system check is a simple check of repeatability to make sure that the system works correctly at the time of the compliance test. It is not a verification of the system with respect to external standards. The SAR system check should detect possible short term drift and errors in the system.

The SAR system check is a complete 1 g or 10 g averaged SAR measurement in a simplified test system with a standard source. The instrumentation and procedures are the same as those used for the compliance tests. The SAR system check has been performed using the specified tissue-equivalent liquid and at a chosen fixed frequency that is within ± 10% of the compliance test mid-band frequency. The system check is performed prior to compliance tests and the result have been checked against the requirements (IEEE1528 and CENELEC Standards) and must always be within ±10% of the target value corresponding to the test frequency, liquid and the source used mentioned in these standards.

The following measurement setup has been used for performing SAR system checks using a box phantoms is based on the procedures fully described in IEEE1528. This SAR System Check is performed at the start of each measurement at a specific frequency range , with appropriate simulant liquids.

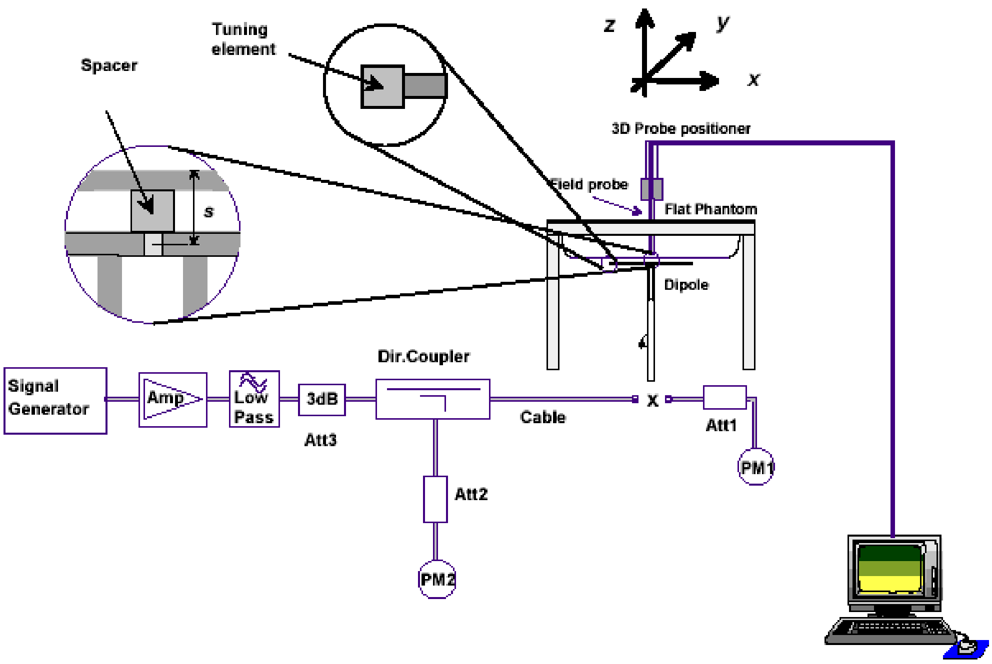

Fig. 10.2.1

With the Signal Generator, Amplifier and directional coupler in place, the source signal has been set up at the relevant frequency and a power meter has been used to measure the power at the end of the SMA cable which is going to be connected to the balanced dipole. The low noise and distortion Signal Generator is adjusted so, that including all cable losses and other losses, the power at the connector X (to be connected to the balanced dipole) is 0.25W (24 dBm) (Reading on PM1 in figure 10.2.1).A calibrated attenuator (Att 1. 20 dB) is used to protect overloading of the Power meter.

No tuning of the balanced dipole was required because fixed tuned and calibrated balanced dipoles for the appropriate test frequencies were used.

10.3 5.8 GHz system check.

For 5.8 GHz validation, a waveguide method as proposed by Li, Ghandi and Kang, 'An open ended waveguide system validation and/or probe calibration for frequencies above 3 GHz, submitted to the IEEE transactions on Microwave Theory and Techniques, June 2003.
The description of this method is taken from 'SARA2 system validation at 5.2 and 5.8 GHz, MI Manning, Indexsar Ltd., 17 October 2003.

SARA2 SYSTEM VALIDATION AT 5.2 AND 5.8GHz

MI Manning, Indexsar Ltd.
17th October 2003.

10.3.1 Introduction.

Whilst international standards recommend techniques for performing system validations of SAR test systems for frequencies between 300MHz and 3GHz, proposals for validation testing at higher frequencies are only at an early-draft stage of discussion.

However, 5 GHz devices are on the market and need to be tested now. IEC62209 has circulated two drafts of proposed procedures for 5-6GHz SAR testing (Annex X), but the procedures are, as yet, ill-defined. The Annex X validation defines a small dipole as a source. Dimensions were incompletely specified in the first draft and are only more fully-defined in the second draft. No recommended separation distance for the dipole beneath the phantom is given in either draft to correspond with the computed reference values suggested.

Indexsar built some dipoles based on the first draft dimensions, but has found that use of these dipoles at the expected 10mm spacing from the liquid do not give results that match the reference values. 5.8GHz validation results for max. 1g SAR with our prototype dipoles were 30% low at a spacing of 10mm and 50% high at a spacing of 7.5mm.

Since then, two useful contributions on 5 GHz validation testing have been circulated. A paper by Li, Gandhi and Kang [1] observes that "It is very difficult to develop half-wave dipole antennas for use in the 5.1 to 5.8 GHz band . . . .". They propose an alternative procedure using an open-ended waveguide placed close to the bottom of the phantom. They propose that the open end of a WR187 waveguide is placed 10mm from the phantom liquid and they present FDTD computation results for use as reference values.

This particular waveguide has different internal dimensions to one recommended for probe calibration purposes in Annex X (WG13), which is unfortunate as otherwise the same waveguide could be recommended for both purposes.

The Utah paper [1] used liquids with the following properties for validations at 5.25 and 5.8 GHz:

Frequency (GHz)	Relative permittivity	Conductivity (S/m)
5.25	48.8	6.82
5.8	46.9	7.83

These property values are not very close to those recommended for compliance evaluations in Annex X, which are:

Frequency (GHz)	Relative permittivity	Conductivity (S/m)
5.25	36.0	4.7
5.8	35.3	5.3

In a separate paper [2], Utah authors argue that results of 1g SAR measurements are not very sensitive to liquid properties at 5-6GHz and use this contention to justify the use of liquids with different properties.

Another paper recently circulated from Motorola personnel makes recommendations for SAR zoom scan measurement grids at 5-6GHz [3]. The authors conclude that noise due to low measured values will compromise 10g volume average calculations and they recommend a restricted size zoom volume for 1g SAR determinations. They also conclude that 4th order polynomial extrapolations are not the best for these frequencies and suggest 3rd order polynomials or fitting to the logarithm of the SAR data.

10.3.2 Validation results using WR187 waveguide.

It would seem that an open-ended waveguide has some advantages in use as a source and we have performed validations based on the recommendations in [1]. The scanning parameters were set as per the recommendations in [3] and 3rd-order polynomial extrapolations were used instead of 4th order. The liquids have rather different property values to those employed in [1], but [2] suggests that this may not affect the max. 1g SAR results by much.

Using these conditions and with use of a WR187 waveguide, validation testing with the following liquid properties resulted in 1g SAR measurements close to the reference values given in [1]. The results are summarized below:

Frequency (GHz)	Relative permittivity	Conductivity (S/m)
5.2	37.12	5.01
5.8	35.41	5.79

Frequency (GHz)	Reference 1g SAR value (W/kg) from [1] normalized to 1W	Measured 1g SAR value (W/kg) / error (%)
5.25	35.80	34.82 (-3%)
5.8	39.46	43.08 (+9%)

Based on the testing performed, it is recommended that SARA2 systems are validated using the open-ended WR187 waveguide technique until improved procedures become available or specific methods become adopted in the relevant standards.

10.3.3 An alternative open-ended waveguide geometry.

It is not clear why [1] recommends a spacing of 10mm from the liquid from a waveguide, when contact with the phantom would seem to be more appropriate and offer more accurate positioning. Also, a matching window with permittivity similar to that of the phantom wall material could minimize reflective losses. Lastly, a waveguide of the same dimensions as that recommended for probe calibration would be a useful reduction in the required equipment budget.

For these reasons, we are commissioning FDTD computations of reference values expected with a WG13 waveguide with a matching window as per Annex X in contact with a 2mm wall phantom filled with a liquid with the properties proposed in Annex X. In this way, we hope to have an optimized validation solution for 5-6GHz testing.

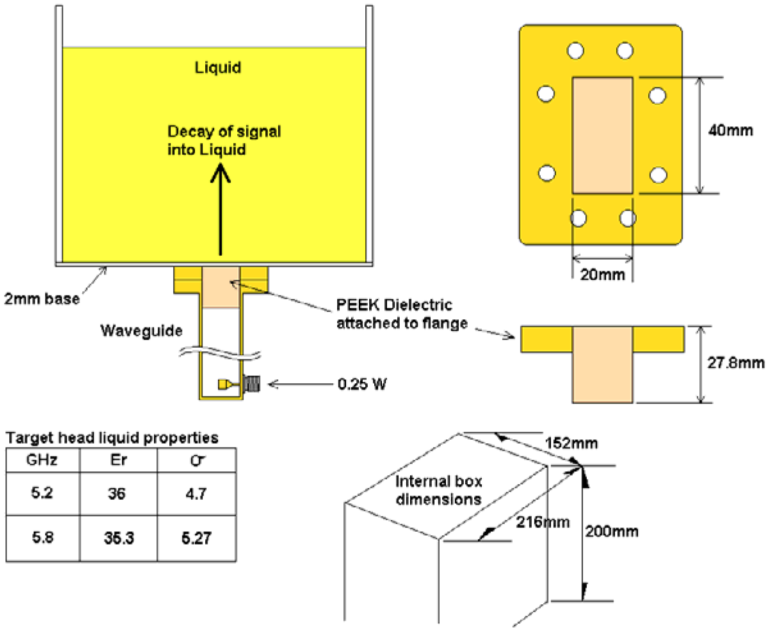

Figure 1: Proposed validation configuration with waveguide in contact with phantom for which reference values will be calculated

References

[1] Q Li, OP Gandhi, G Kang, 'An open-ended waveguide system validation and/or probe calibration for frequencies above 3GHz', submitted to IEEE Transactions on Microwave Theory and Techniques, June 2003.

[2] G Kang & OP Gandhi, 'Effect of dielectric properties on the peak 1- and 10g SAR for 802.11 a/b/g frequencies of 2.45 and 5.15 to 5.85 GHz', to be published in IEEE Transactions on Electromagnetic Compatibility.

[3] Recommendations for SAR zoom scan measurement grids at 5-6GHz.

10.4 Dielectric property measurement of tissue-simulant liquids for SAR testing.

10.4.1 Introduction.

This section describes the measurement of the dielectric properties of tissue-equivalent material as part of the SAR characterization procedure and the method used.

The measurement method is based on a published technique *(Toropainen et al , 'Method for accurate measurement of complex permittivity of tissue equivalent liquids', Electronics Letters 36 (1) 2000 pp32-34)* and uses a fixture with 2 parallel planes with a conductor in between. Liquid filling the space between the planes immerses the inner conductor wholly. Measurements of S_{21} with an empty fixture and that of a filled fixture are conducted so that the complex dielectric properties of the fluid can be deduced. The fixture is also referred to as *TEM line.*

10.4.2 TEM-cell construction.

The TEM cell construction is shown in Figure 10.3.1 and consists of a central cylindrical transmission line sandwiched between two ground planes

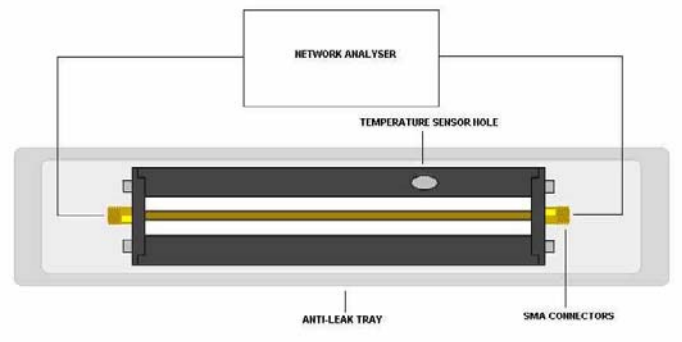

Figure 10.3.1. TEM Cell Construction.

Four different sensors can be used with transmission line lengths of 30mm, 60mm, 80mm and 160mm. The transmission line is terminated with SMA connectors at either end using short 50 ohm launcher sections. The assembly is held firmly against a plastic base with a clamping arrangement providing a seal to retain the liquid. The liquid under test is introduced with a pipette to fill the space between the ground planes. Care has been taken to prevent air bubbles and this is particularly important with viscous liquids. A hole is provided in one of the ground planes so that a thermometer probe has been be inserted to monitor the temperature. The cell is washed out and thoroughly dried before further use.

A vector network analyser (VNA) is used to measure the performance of the cell. A good impedance match will be found when air filled indicating that the transmission line impedance is close to 50 ohm. The transmission loss and phase are measured with and without the liquid to enable the electrical properties to be deduced.

10.4.3 Calculation of dielectric properties from VNA measurements.

The complex permittivity of the simulant liquids were measured using a TEM line sensor as recommended in the EN50361 and draft IEEE1528 standards. The method [1] is based on the measurement of complex transmission coefficient of a TEM-line filled with the liquid. Transmission measurement is done using a VNA, recording the magnitude and phase of scattering coefficient S_{21}. The complex permittivity of the liquid is calculated from the magnitude and phase of S_{21} by numerical solution of the equation of transmission coefficient derived by signal flow graph technique

$$S_{21} = \frac{\left(1-\Gamma^2\right)\exp\left(-\mathrm{j}(k-k_0)d\right)}{1-\Gamma^2\exp\left(-\mathrm{j}2kd\right)},$$

$$\Gamma = \frac{1-\sqrt{\varepsilon_r}}{1+\sqrt{\varepsilon_r}},$$

$$k = \frac{2\pi f}{c_0}\sqrt{\varepsilon_r},$$

where Γ is the reflection coefficient at liquid surfaces, k the propagation factor in the liquid, k_0 the vacuum propagation factor, d the length of the sample, f the frequency and $\varepsilon_r = \varepsilon_r' - j\varepsilon_r''$ the relative complex permittivity of the sample.

10.5 Measurement uncertainty.

10.5.1 Introduction.

A measurement uncertainty assessment has been undertaken following guidance given in EN50361 and IEEE1528. IndexSAR Ltd has supplied a generic uncertainty analysis for the SARA2 system in the form of a spreadsheet and the supporting assessments are documented in an IndexSAR document IXS-2028. Additionally, uncertainties resulting from the probe positioning system and the upright phantom geometry are discussed in additional documents.

Some of the uncertainty contributions are site-specific and, for these, TNO Electronic Products & Services (EPS) has assessed the uncertainty contributions arising from local environmental and procedural factors.

The resultant uncertainty budget is shown on the next pages.

10.5.2 Uncertainty calculated for IEEE1528 : standard measurements (2450 MHz).

a	*b*	*c*	*d*	*e= f(d,k)*	*f*	*g*	*h= cxg/e*	*i= cxg/e*	*k*
Uncertainty Component	Section	Tol. (± %)	Prob. Dist.	Div.	ci (1-g)	ci (10-g)	1-g ui (±%)	10-g ui (±%)	vt
Measurement System									
Probe Calibration	E2.1	10.0	N	1or k	1	1	5.0	5.0	∞
Axial Isotropy	E2.2	5.93	R	√3	0.7	0.7	2.4	2.4	∞
Hemispherical Isotropy	E2.2	10.92	R	√3	1	1	6.3	6.3	∞
Boundary Effect	E2.3	4.0	R	√3	1	1	2.3	2.3	∞
Linearity	E2.4	0.93	R	√3	1	1	0.5	0.5	∞
System Detection Limits	E2.5	1.0	R	√3	1	1	0.6	0.6	∞
Readout Electronics	E2.6	1.0	N	1or k	1	1	1.0	1.0	∞
Response Time	E2.7	0.0	R	√3	1	1	0.0	0.0	∞
Integration Time	E2.8	1.8	R	√3	1	1	1.0	1.0	∞
RF Ambient Conditions	E6.1	3.0	R	√3	1	1	1.7	1.7	∞
Probe Positioner Mechanical Tolerance	E6.2	0.6	R	√3	1	1	0.3	0.3	∞
Probe Positioning wrt Phantom Shell	E6.3	5.0	R	√3	1	1	2.9	2.9	∞
SAR Evaluation Algoritms	E5.2	8.0	R	√3	1	1	4.6	4.6	∞
Test sample Related									∞
Test Sample Positioning	E4.2	5.0	R	√3	1	1	2.9	2.9	∞
Device Holder Uncertainty	E4.1	3	R	√3	1	1	1.7	1.7	∞
Output Power Variation	6.6.2	5.0	R	√3	1	1	2.9	2.9	∞
Phantom and Tissue Parameters									∞
Phantom Uncertainty (shape and thickness)	E3.1	4.0	R	√3	1	1	2.3	2.3	∞
Liquid Conductivity Target - tolerance	E3.2	1.0	R	√3	0.7	0.5	0.4	0.3	∞
Liquid Conductivity - measurement uncert.	E3.3	4.7	R	√3	0.7	0.5	1.9	1.4	∞
Liquid Permittivity Target tolerance	E3.2	4.4	R	√3	0.6	0.5	1.5	1.3	∞
Liquid Permittivity - measurement uncert.	E3.3	3.3	R	√3	0.6	0.5	1.1	1.0	∞
Combined Standard Uncertainty		$u_c = \sqrt{\sum_{i=1}^{m} c_i^2 \cdot u_i^2}$					11.7	11.6	
Expanded Uncertainty (95% confidence interval)	Normal k=1.96 **ue=k* u_c**						**22.9%**	**22.7%**	

10.5.3 Uncertainty calculated for IEEE1528 : standard measurements (5800 MHz).

a	*b*	*c*	*d*	*e= f(d,k)*	*f*	*g*	*h= cxg/e*	*i= cxg/e*	*k*
Uncertainty Component	Section	Tol. (± %)	Prob. Dist.	Div.	ci (1-g)	ci (10-g)	1-g ui (±%)	10-g ui (±%)	vt
Measurement System									
Probe Calibration	E2.1	12.0	N	1or k	1	1	6.0	6.0	∞
Axial Isotropy	E2.2	5.93	R	√3	0.7	0.7	2.4	2.4	∞
Hemispherical Isotropy	E2.2	10.92	R	√3	1	1	6.3	6.3	∞
Boundary Effect	E2.3	4.0	R	√3	1	1	2.3	2.3	∞
Linearity	E2.4	0.93	R	√3	1	1	0.5	0.5	∞
System Detection Limits	E2.5	1.0	R	√3	1	1	0.6	0.6	∞
Readout Electronics	E2.6	1.0	N	1or k	1	1	1.0	1.0	∞
Response Time	E2.7	0.0	R	√3	1	1	0.0	0.0	∞
Integration Time	E2.8	1.8	R	√3	1	1	1.0	1.0	∞
RF Ambient Conditions	E6.1	3.0	R	√3	1	1	1.7	1.7	∞
Probe Positioner Mechanical Tolerance	E6.2	0.6	R	√3	1	1	0.3	0.3	∞
Probe Positioning wrt Phantom Shell	E6.3	5.0	R	√3	1	1	2.9	2.9	∞
SAR Evaluation Algoritms	E5.2	8.0	R	√3	1	1	4.6	4.6	∞
Test sample Related									∞
Test Sample Positioning	E4.2	10.0	R	√3	1	1	5.8	5.8	∞
Device Holder Uncertainty	E4.1	5.0	R	√3	1	1	2.9	2.9	∞
Output Power Variation	6.6.2	5.0	R	√3	1	1	2.9	2.9	∞
Phantom and Tissue Parameters									∞
Phantom Uncertainty (shape and thickness)	E3.1	4.0	R	√3	1	1	2.3	2. 3	∞
Liquid Conductivity Target - tolerance	E3.2	7.5	R	√3	0.7	0.5	3.0	2.2	∞
Liquid Conductivity - measurement uncert.	E3.3	5.0	R	√3	0.7	0.5	2.0	1.4	∞
Liquid Permittivity Target tolerance	E3.2	1.0	R	√3	0.7	0.5	0.4	0.3	∞
Liquid Permittivity - measurement uncert.	E3.3	3.3	R	√3	0.7	0.5	1.3	1.0	∞
Combined Standard Uncertainty		$u_c = \sqrt{\sum_{i=1}^{m} c_i^2 \cdot u_i^2}$					13.5	13.3	
Expanded Uncertainty (95% confidence interval)		Normal k=1.96 **ue=k* u_c**					**26.5%**	**26.1%**	

10.5.4 Uncertainty calculated for IEEE1528 : System performance check (2450 MHz).

a	*b*	*c*	*d*	*e= f(d,k)*	*f*	*g*	*h= cxg/e*	*i= cxg/e*	*k*
Uncertainty Component	Section	Tol. (± %)	Prob. Dist.	Div.	ci (1-g)	ci (10-g)	1-g ui (±%)	10-g ui (±%)	vt
Measurement System									
Probe Calibration	E2.1	10.0	N	1or k	1	1	5.0	5.0	∞
Axial Isotropy	E2.2	5.93	R	√3	0.7	0.7	2.4	2.4	∞
Hemispherical Isotropy	E2.2	10.92	R	√3	1	1	6.3	6.3	∞
Boundary Effect	E2.3	4.0	R	√3	1	1	2.3	2.3	∞
Linearity	E2.4	0.93	R	√3	1	1	0.5	0.5	∞
System Detection Limits	E2.5	1.0	R	√3	1	1	0.6	0.6	∞
Readout Electronics	E2.6	1.0	N	1or k	1	1	1.0	1.0	∞
Response Time	E2.7	0.0	R	√3	1	1	0.0	0.0	∞
Integration Time	E2.8	1.8	R	√3	1	1	1.0	1.0	∞
RF Ambient Conditions	E6.1	3.0	R	√3	1	1	1.7	1.7	∞
Probe Positioner Mechanical Tolerance	E6.2	0.6	R	√3	1	1	0.3	0.3	∞
Probe Positioning wrt Phantom Shell	E6.3	5.0	R	√3	1	1	2.9	2.9	∞
SAR Evaluation Algoritms	E5.2	8.0	R	√3	1	1	4.6	4.6	∞
Dipole Related									∞
Dipole axis to liquid distance	8, E4.2	1.0	R	√3	1	1	0.6	0.6	∞
Input Power & SAR Drift measurments	8, 6.6.2	1.5	R	√3	1	1	0.9	0.9	∞
Phantom and Tissue Parameters									∞
Phantom Uncertainty (shape and thickness)	E3.1	4.0	R	√3	1	1	2.7	2. 7	∞
Liquid Conductivity Target - tolerance	E3.2	1.0	R	√3	0.7	0.5	0.4	0.3	∞
Liquid Conductivity - measurement uncert.	E3.3	4.7	R	√3	0.7	0.5	1.9	1.4	∞
Liquid Permittivity Target tolerance	E3.2	4.4	R	√3	0.6	0.5	1.5	1.3	∞
Liquid Permittivity - measurement uncert.	E3.3	3.3	R	√3	0.6	0.5	1.1	1.0	∞
Combined Standard Uncertainty		$u_c = \sqrt{\sum_{i=1}^{m} c_i^2 \cdot u_i^2}$					10.9	10.8	
Expanded Uncertainty (95% confidence interval)	Normal k=1.96 **ue=k* u_c**						**21.3%**	**21.1%**	

10.5.5 Uncertainty calculated for IEEE1528 : System performance check (5800 MHz).

a	*b*	*c*	*d*	*e= f(d,k)*	*f*	*g*	*h= cxg/e*	*i= cxg/e*	*k*
Uncertainty Component	Section	Tol. (± %)	Prob. Dist.	Div.	ci (1-g)	ci (10-g)	1-g ui (±%)	10-g ui (±%)	vt
Measurement System									
Probe Calibration	E2.1	12.0	N	1or k	1	6.0	6.0	6.0	∞
Axial Isotropy	E2.2	5.93	R	√3	0.7	2.4	2.4	2.4	∞
Hemispherical Isotropy	E2.2	10.92	R	√3	1	6.3	6.3	6.3	∞
Boundary Effect	E2.3	4.0	R	√3	1	2.3	2.3	2.3	∞
Linearity	E2.4	0.93	R	√3	1	0.5	0.5	0.5	∞
System Detection Limits	E2.5	1.0	R	√3	1	0.6	0.6	0.6	∞
Readout Electronics	E2.6	1.0	N	1or k	1	1.0	1.0	1.0	∞
Response Time	E2.7	0.0	R	√3	1	0.0	0.0	0.0	∞
Integration Time	E2.8	1.8	R	√3	1	1.0	1.0	1.0	∞
RF Ambient Conditions	E6.1	3.0	R	√3	1	1.7	1.7	1.7	∞
Probe Positioner Mechanical Tolerance	E6.2	0.6	R	√3	1	0.3	0.3	0.3	∞
Probe Positioning wrt Phantom Shell	E6.3	5.0	R	√3	1	2.9	2.9	2.9	∞
SAR Evaluation Algorithms	E5.2	8.0	R	√3	1	4.6	4.6	4.6	∞
Dipole Related									∞
Dipole axis to liquid distance	8, E4.2	1.0	R	√3	1	1	7.5	7.5	∞
Input Power & SAR Drift measurements	8, 6.6.2	2.0	R	√3	1	1	2.89	2.89	∞
Phantom and Tissue Parameters									∞
Phantom Uncertainty (shape and thickness)	E2.1	4.0	R	√3	1	1	2.3	2. 3	∞
Liquid Conductivity Target - tolerance	E2.2	7.5	R	√3	0.7	0.5	3.0	2.2	∞
Liquid Conductivity - measurement uncert.	E2.2	5.0	R	√3	0.7	0.5	2.0	1.4	∞
Liquid Permittivity Target tolerance	E2.2	1.0	R	√3	0.7	0.5	0.4	0.3	5
Liquid Permittivity - measurement uncert.	E2.2	3.3	R	√3	0.7	0.5	1.3	1.0	∞
Combined Standard Uncertainty		$u_c = \sqrt{\sum_{i=1}^{m} c_i^2 \cdot u_i^2}$					11.0	10.9	
Expanded Uncertainty (95% confidence interval)		Normal k=1.96 **ue=k* u_c**					**21.5%**	**21.3%**	

11 List of utilized test equipment.

Inventory number	Description	Brand	Model
03012	Network Analyzer (VNA)	Rohde & Schwarz	ZVC
03013	VNA Calibration Kit	Rohde & Schwarz	
12483	Guidehorn	EMCO	3115
12484	Guidehorn	EMCO	3115
12488	Guidehorn 18 - 26.5 GHz	EMCO	RA42-K-F-4B-C
12533	Signalgenerator	MARCONI	2032
12559	Digital storage oscilloscope	Le Croy	9310M
12561	DC Power Supply 20A/70V	DELTA	SM7020D
12605	calibrated dipole 28MHz-1GHz	Emco	3121c
12608	HF milliwattmeter	Hewlett Packard	HP435a
12609	Power sensor 10MHz-18GHz	Hewlett Packard	HP8481A
3664	Spectrum analyzer	HP	HP8593E
13078	Preamplifier 0.1 GHz - 12 GHz	Miteq	AMF-3D-001120-35-4p
13526	Signalgenerator 20 GHz	Hewlett & Packard	83620A
13594	Preamplifier 10 GHz - 25 GHz	Miteq	AMF-6D-100250-10p
14450	2.4 GHz bandrejectfilter	BSC	XN-1783
99068	Detector N-F/BNC-F	Radiall	R451576000
99076	Bandpassfilter 4 - 10 GHz	Reactel	7AS-7G-6G-511
99112	Tripod	Chase	--
99136	Bandpassfilter 10 - 26.5 GHz	Reactel	9HS-10G/26.5G-S11
03011	RF Amplifier (1 Watt)	IndexSAR	
03010	Bench-top Robot	Mitsubishi	RV-E2
03009	Calibration dipole 2450	IndexSAR	IXD 0022
03008	Calibration dipole 5800	IndexSAR	
03007	Directional Coupler	Hewlett & Packard	779D
03006	Attenuator (3 dB)	Hewlett & Packard	
03005	Hygrometer/room temperature meter		
03004	SAR Probe	IndexSAR	S/N 0131
03003	Phantom box	IndexSAR	N.A.
03002	TEM line liquid measurement	IndexSAR	N.A.
03012	Waveguide W-137	IndexSAR	N.A.
03013	Calibrated mercury thermometers	NMI	15-30 C

12 Test software.

During the tests as indicated in this test report the TNO EPS SARA2 system was operated with:

SARA2 system v2.3VPM
Mitsubishi robot controller firmware revision RV-E2 Version C9a
IXA-10 Probe amplifier Version 2.4
DiLine Dielectric Kit Software v 0.109 (12/6/2003)

Indexsar Limited
Oakfield House
Cudworth Lane
Newdigate
Surrey RH5 5DR
Tel: +44 (0) 1306 631 233
Fax: +44 (0) 1306 631 834
e-mail: enquiries@indexsar.com

Calibration Certificate
Dosimetric E-field Probe

Type:	**IXP-050**
Manufacturer:	**IndexSAR, UK**
Serial Number:	**0131**
Place of Calibration:	**IndexSAR, UK**

IndexSAR Limited hereby declares that the IXP-050 Probe named above has been calibrated for conformity to the IEEE 1528 and CENELEC En 50361 standards on the date shown below.

Date of Initial Calibration:	**1st October 2003**

The probe named above will require a calibration check on the date shown below.

Next Calibration Date:	**October 2004**

The calibration was carried out using the methods described in the calibration document. Where applicable, the standards used in the calibration process are traceable to the UK's National Physical Laboratory.

Calibrated By: [signature]

Approved By: [signature]

<u>Please keep this certificate with the calibration document. When the probe is sent for a calibration check, please include the calibration document.</u>

IMMERSIBLE SAR PROBE

CALIBRATION REPORT

Part Number: IXP – 050

S/N 0131

1st October 2003

Indexsar Limited
Oakfield House
Cudworth Lane
Newdigate
Surrey RH5 5DR
Tel: +44 (0) 1306 631 233
Fax: +44 (0) 1306 631 834
e-mail: enquiries@indexsar.com

INTRODUCTION

This Report presents measured calibration data for a particular Indexsar SAR probe (S/N 0131) and describes the procedures used for characterisation and calibration.

Indexsar probes are characterised using procedures that, where applicable, follow the recommendations of CENELEC [1] and IEEE [2] standards. The procedures incorporate techniques for probe linearisation, isotropy assessment and determination of liquid factors (conversion factors). Calibrations are determined by comparing probe readings with analytical computations in canonical test geometries (waveguides) using normalised power inputs.

Each step of the calibration procedure and the equipment used is described in the sections below.

CALIBRATION PROCEDURE

1. Equipment Used

For the first part of the characterisation procedure, the probe is placed in an isotropy measurement jig as pictured in Figure 1. In this position the probe can be rotated about its axis by a non-metallic belt driven by a stepper motor.

The probe is attached via its amplifier and an optical cable to a PC. A schematic representation of the test geometry is illustrated in Figure 2.

A balanced dipole (900 MHz) is inserted horizontally into the bracket attached to a second belt (Figure 1). The dipole can also be rotated about its axis. A cable connects the dipole to a signal generator, via a directional coupler and power meter. The signal generator feeds an RF amplifier at constant power, the output of which is monitored using the power meter. The probe is positioned so that its sensors line up with the rotation center of the source dipole. By recording output voltage measurements of each channel as both the probe and the dipole are rotated, data are obtained from which the spherical isotropy of the probe can be optimised and its magnitude determined.

The calibration process requires E-field measurements to be taken in air, in 900 MHz simulated brain liquid and at other frequencies/liquids as appropriate.

2. Linearising probe output

The probe channel output signals are linearised in the manner set out in Refs [1] and [2]. The following equation is utilized for each channel:

$$U_{lin} = U_{o/p} + U_{o/p}^{\ 2} / DCP \qquad (1)$$

where U_{lin} is the linearised signal, $U_{o/p}$ is the raw output signal in voltage units and DCP is the diode compression potential in similar voltage units.

DCP is determined from fitting equation (1) to measurements of U_{lin} versus source feed power over the full dynamic range of the probe. The DCP is a characteristic of the schottky diodes used as the sensors. For the IXP-050 probes with CW signals the DCP values are typically 0.10V (or 20 in the voltage units used by Indexsar software, which are V*200).

3. Selecting channel sensitivity factors to optimise isotropic response

The basic measurements obtained using the calibration jig (Fig 1) represent the output from each diode sensor as a function of the presentation angle of the source (probe and dipole rotation angles). The directionality of the orthogonally-arranged sensors can be checked by analysing the data using dedicated Indexsar software, which displays the data in 3D format as in Figure 3. The left-hand side of this diagram shows the individual channel outputs after linearisation (see above). The program uses these data to balance the channel outputs and then applies an optimisation process, which makes fine adjustments to the channel factors for optimum isotropic response.

The next stage of the process is to calibrate the Indexsar probe to a W&G EMR300 E-field meter in air. The principal reasons for this are to obtain conversion factors applicable should the probe be used in air and to provide an overall measure of the probe sensitivity.

A multiplier is applied to factors to bring the magnitudes of the average E-field measurements as close as possible to those of the W&G probe.

The following equation is used (where linearised output voltages are in units of V*200):

$$E_{air}^2\ (V/m) = U_{linx} * \text{Air Factor}_x + U_{liny} * \text{Air Factor}_y + U_{linz} * \text{Air Factor}_z \quad (2)$$

It should be noted that the air factors are not separately used for normal SAR testing. The IXP-050 probes are optimised for use in tissue-simulating liquids and do not behave isotropically in air.

4. 900 MHz Liquid Calibration

Conversion factors for use when the probes are immersed in tissue-simulant liquids at 900 MHz are determined either using a waveguide or by comparison to a reference probe that has been calibrated by NPL. Waveguide procedures are described later. The summary sheet indicates the method used for the probe S/N 0131.

The conversion factor, referred to as the 'liquid factor' is also applied to the measurements of each channel. The following equation is used (where output voltages are in units of V*200):

$$E_{liq}^2\ (V/m) = U_{linx} * \text{Air Factor}_x * \text{Liq Factor}_x + U_{liny} * \text{Air Factor}_y * \text{Liq Factor}_y + U_{linz} * \text{Air Factor}_z * \text{Liq Factor}_z \quad (3)$$

A 3D representation of the spherical isotropy for probe S/N 0131 using these factors is shown in Figure 3.

The rotational isotropy can also determined from the calibration jig measurements and is reported as the 900MHz isotropy in the summary table. Note that waveguide measurements can also be used to determine rotational isotropy (Fig. 5).

The design of the cells used for determining probe conversion factors are waveguide cells is shown in Figure 4. The cells consist of a coax to waveguide transition and an open-ended section of waveguide containing a dielectric separator. Each waveguide cell stands in the upright positition and is filled with liquid within 10 mm of the open end. The seperator provides a liquid seal and is designed for a good electrical transition from air filled guide to liquid filled guide. The choice of cell depends on the portion of the frequency band to be examined and the choice of liquid used. The depth of liquid ensures there is negligible radiation from the waveguide open top and that the probe calibration is not influenced by reflections from nearby objects. The return loss at the coaxial connector of the filled waveguide cell is measured initially using a network analyser and this information is used subsequently in the calibration procedure. The probe is positioned in the centre of the waveguide and is adjusted vertically or rotated using stepper motor arrangements. The signal generator is connected to the waveguide cell and the power is monitored with a coupler and a power meter. A fuller description of the waveguide method is given below.

The liquid dielectric parameters used for the probe calibrations are listed in the Tables below. The final calibration factors for the probe are listed in the summary chart.

WAVEGUIDE MEASUREMENT PROCEDURE

The calibration method is based on setting up a calculable specific absorption rate (SAR) in a vertically-mounted WG8 (R22) waveguide section [1]. The waveguide has an air-filled, launcher section and a liquid-filled section separated by a matching window that is designed to minimise reflections at the liquid interface. A TE_{01} mode is launched into the waveguide by means of a N-type-to-waveguide adapter. The power delivered to the liquid section is calculated from the forward power and reflection coefficient measured at the input to the waveguide. At the centre of the cross-section of the waveguide, the local spot SAR in the liquid as a function of distance from the window is given by functions set out in IEEE1528 as below:

Because of the low cutoff frequency, the field inside the liquid nearly propagates as a TEM wave. The depth of the medium (greater than three penetration depths) ensures that reflections at the upper surface of the liquid are negligible. The power absorbed in the liquid is determined by measuring the waveguide forward and reflected power. Equation (4) shows the relationship between the SAR at the cross-sectional center of the lossy waveguide and the longitudinal distance (z) from the dielectric separator

$$SAR(z) = \frac{4\left(P_f - P_b\right)}{\rho ab\delta} e^{-2z/\delta} \tag{4}$$

where the density ρ is conventionally assumed to be 1000 kg/m^3, ab is the cross-sectional area of the waveguide, P_f and P_b are the forward and reflected power inside the lossless section of the waveguide, respectively. The penetration depth δ, which is the reciprocal of the waveguide-mode attenuation coefficient, is determined from a scan along the z-axis and compared with the theoretical value determined from Equation (5) using the measured dielectric properties of the lossy liquid.

$$\delta = \left[\mathrm{Re}\left\{ \sqrt{(\pi / a)^2 + j\omega\mu_o\left(\sigma + j\omega\varepsilon_o\varepsilon_r\right)} \right\} \right]^{-1} . \quad (5)$$

Table A.1 of [1] can be used for designing calibration waveguides with a return loss greater than 30 dB at the most important frequencies used for personal wireless communications. Values for the penetration depth for these specific fixtures and tissue-simulating mixtures are also listed in Table A.1.

According to [1], this calibration technique provides excellent accuracy, with standard uncertainty of less than 3.6% depending on the frequency and medium. The calibration itself is reduced to power measurements traceable to a standard calibration procedure. The practical limitation to the frequency band of 800 to 2500 MHz because of the waveguide size is not severe in the context of compliance testing.

CALIBRATION FACTORS MEASURED FOR PROBE S/N 0131

The probe was calibrated at 900, 1800, 1900 and 2450MHz MHz in liquid samples representing both brain liquid and body fluid at these frequencies. The calibration was for CW signals only, and the axis of the probe was parallel to the direction of propagation of the incident field i.e. end-on to the incident radiation. The axial isotropy of the probe was measured by rotating the probe about its axis in 10 degree steps through 360 degrees in this orientation.

The reference point for the calibration is in the centre of the probe's cross-section at a distance of 2.7 m from the probe tip in the direction of the probe amplifier. A value of 2.7 mm should be used for the tip to sensor offset distance in the software.

It is important that the diode compression point and air factors used in the software are the same as those quoted in the results tables, as these are used to convert the diode output voltages to a SAR value.

DIELECTRIC PROPERTIES OF LIQUIDS

The dielectric properties of the brain and body tissue-simulant liquids employed for calibration are listed in the tables below. The measurements were performed prior to each waveguide test using an Indexsar DiLine measurement kit, which uses the TEM method as recommended in [2].

AMBIENT CONDITIONS

Measurements were made in the open laboratory at 22 $\pm$ 2.0°C. The temperature of the liquids in the waveguide used was measured using a mercury thermometer.

RESPONSE TO MODULATED SIGNALS

To measure the response of the probe and amplifier to modulated signals, the probe is held vertically in a liquid-filled waveguide.

An RF amplifier is allowed to warm up and stabilise before use. A spectrum analyser is used to demonstrate that the peak power of the RF amplifier for the CW signals and the pulsed signals are within 0.1dB of each other when the signal generator is switched from CW to modulated output. Subsequently, the power levels recorded are read from a power meter when a CW signal is being transmitted.

The test sequence involves manually stepping the power up in regular (e.g. 2 dB) steps from the lowest power that gives a measurable reading on the SAR probe up to the maximum that the amplifiers can deliver.

At each power level, the individual channel outputs from the SAR probe are recorded at CW and then recorded again with the modulation setting. The results are entered into a spreadsheet. Using the spreadsheets, the modulated power is calculated by applying a factor to the measured CW power (e.g. for GSM, this factor is 9.03dB). This process is repeated 3 times with the response maximised for each channel sensor in turn.

The probe channel output signals are linearised in the manner set out in Section 1 above using equation (1) with the DCPs determined from the linearisation procedure. Calibration factors for the probe are used to determine the E-field values corresponding to the probe readings using equation (3). SAR is determined from the equation

$$SAR\ (W/kg) = E_{liq}^2\ (V/m) * \sigma(S/m) / 1000 \qquad (6)$$

Where σ is the conductivity of the simulant liquid employed.

Using the spreadsheet data, the DCP value for linearising each of the individual channels (X, Y and Z) is assessed separately. The corresponding DCP values are listed in the summary page of the calibration factors for each probe.

Figure 7 shows the linearised probe response to GSM signals, Figure 8 the response to GPRS signals (GSM with 2 timeslots) and Figure 9 the response to CDMA IS-95A and W-CDMA signals.

Additional tests have shown that the modulation response is similar at 1800MHz and is not affected by the orientation between the source and the probe.

VPM (Virtual Probe Miniaturisation)

SAR probes with 3 diode-sensors in an orthogonal arrangement are designed to display an isotropic response when exposed to a uniform field. However, the probes are ordinarily used for measurements in non-uniform fields and isotropy is not assured when the field gradients are significant compared to the dimensions of the tip containing the three orthogonally-arranged dipole sensors.

It becomes increasingly important to assess the effects of field gradients on SAR probe readings when higher frequencies are being used. For Indexsar IXP-050 probes, which are of 5mm tip diameter, field gradient effects are minor at GSM frequencies, but are major above 5GHz. Smaller probes are less affected by field gradients and so probes, which are significantly less than 5mm diameter, would be better for applications above 5GHz.

The IndexSAR report IXS0223 describes theoretical and experimental studies to evaluate the issues associated with the use of probes at arbitrary angles to surfaces and field directions. Based upon these studies, the procedures and uncertainty analyses referred to in P1528 are addressed for the full range of probe presentation angles.

In addition, generalized procedures for correcting for the finite size of immersible SAR probes are developed. Use of these procedures enables application of schemes for virtual probe miniaturization (VPM) – allowing probes of a specific size to be used where physically-smaller probes would otherwise be required.

Given the typical dimensions of 3-channel SAR probes presently available, use of the VPM technique extends the satisfactory measurement range to higher frequencies.

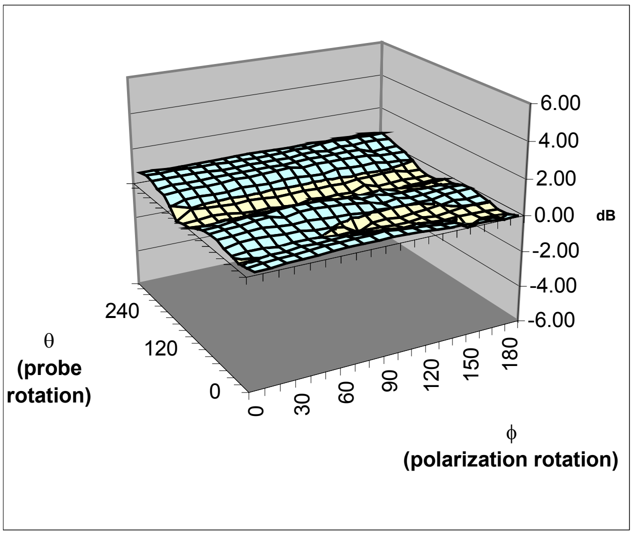

Surface Isotropy diagram of IXP-050 Probe S/N 0131 at 2450MHz after VPM

Probe tip radius	1.25
X Ch. Angle to red dot	10

	Head		Body	
Frequency	**Bdy. Corrn. – f(0)**	**Bdy. Corrn. – d(mm)**	**Bdy. Corrn. – f(0)**	**Bdy. Corrn. – d(mm)**
835	0.5	2	0.58	2
900	0.5	2	0.61	2
1800	0.62	1	0.2	1
1900	0.6	1	0.5	1
2450	0.6	1	0.65	2
5200	2	1	2	1
5800	0.75	1	1	2

SUMMARY OF CALIBRATION FACTORS FOR PROBE IXP-050 S/N 0131

Spherical isotropy measured at 900 MHz	0.30	(+/-) dB

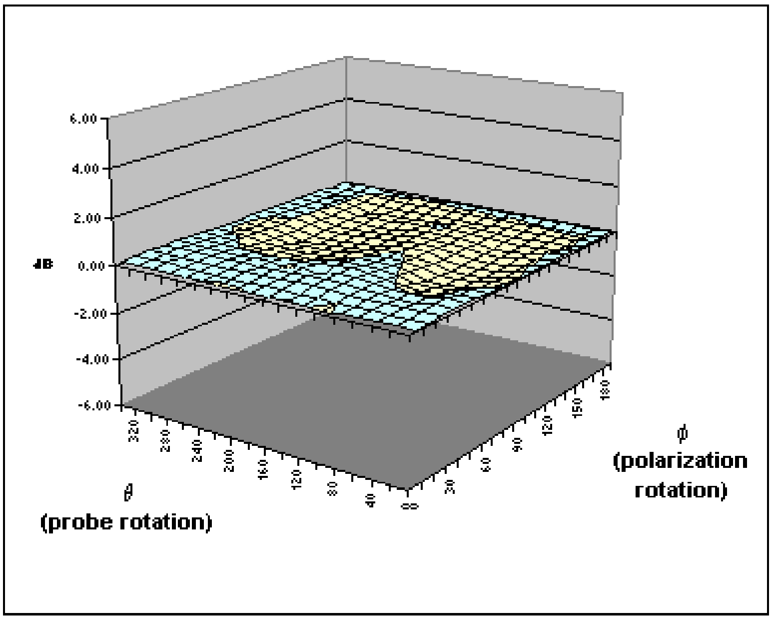

	X	Y	Z	
Air factors	405	461	396	(V*200)
DCPs	20	20	20	(V*200)
GSM	8	6.4	8	(V*200)
CDMA	20	20	20	(V*200)

f (MHz)	Axial isotropy (+/- dB)		SAR conversion factors (liq/air)		Notes
	BRAIN	BODY	BRAIN	BODY	
835	0.17	0.17	0.363	0.399	1,2,3
900	0.19	0.17	0.369	0.408	1,2,3
1800	0.17	0.17	0.462	0.471	1,2,3
1900	0.18	0.18	0.468	0.504	1,2,3
2450	0.18	0.20	0.534	0.540	1,2,3
5200	0.35	0.35	0.480	0.870	1,2
5800	0.35	0.35	0.435	0.750	1,2

Notes	
1)	Calibrations done at 22C +/- 2C
2)	Waveguide calibration
3)	Checked using box-phantom validation test

(the graph shows a simple, spreadsheet representation of surface shown in 3D in Figure 3 below)

PROBE SPECIFICATIONS

Indexsar probe 0131, along with its calibration, is compared with CENELEC and IEEE standards recommendations (Refs [1] and [2]) in the Tables below. A listing of relevant specifications is contained in the tables below:

Dimensions	S/N 0131	CENELEC [1]	IEEE [2]
Overall length (mm)	350		
Tip length (mm)	10		
Body diameter (mm)	12		
Tip diameter (mm)	5.2	8	8
Distance from probe tip to dipole centers (mm)	2.7		

Dynamic range	S/N 0131	CENELEC [1]	IEEE [2]
Minimum (W/kg)	0.01	<0.02	0.01
Maximum (W/kg) N.B. only measured to 35 W/kg	>35	>100	100

Linearity of response	S/N 0131	CENELEC [1]	IEEE [2]
Over range 0.01 – 100 W/kg (+/- dB)	0.125	0.50	0.25

Isotropy (measured at 900MHz)	S/N 0131	CENELEC [1]	IEEE [2]
Axial rotation with probe normal to source (+/- dB) at 835, 900, 1450, 1500, 1800, 1900 and 2450 MHz	Max. 0.35 (see summary table)	0.5	0.25
Spherical isotropy covering all orientations to source (+/- dB)	0.30	1.0	0.50

Construction	Each probe contains three orthogonal dipole sensors arranged on a triangular prism core, protected against static charges by built-in shielding, and covered at the tip by PEEK cylindrical enclosure material. No adhesives are used in the immersed section. Outer case materials are PEEK and heat-shrink sleeving.
Chemical resistance	Tested to be resistant to glycol and alcohol containing simulant liquids but probes should be removed, cleaned and dried when not in use.

REFERENCES

[1] CENELEC, EN 50361, July 2001. Basic Standard for the measurement of specific absorption rate related to human exposure to electromagnetic fields from mobile phones.

[2] IEEE 1528, Recommended practice for determining the spatial-peak specific absorption rate (SAR) in the human body due to wireless communications devices: Experimental techniques.

[3] Calibration report on SAR probe IXP-050 S/N 0071 from National Physical Laboratory. Test Report EF07/2002/03/IndexSAR. Dated 20 February 2002.

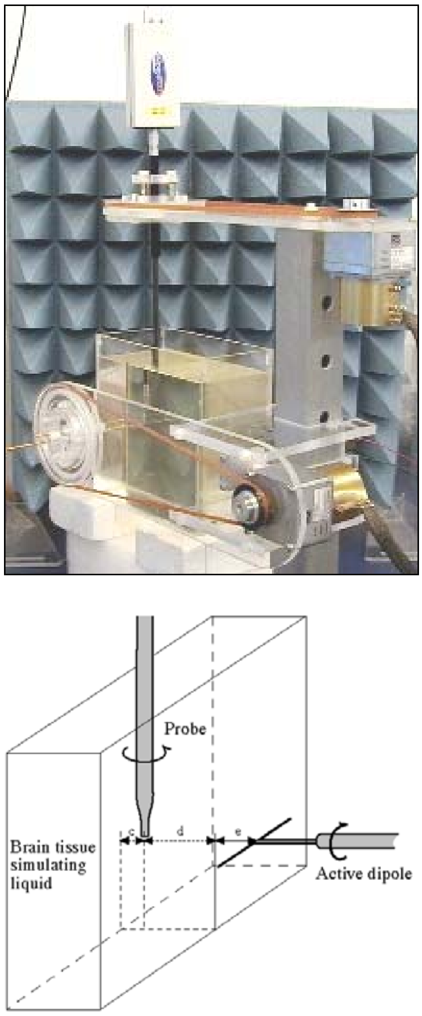

Figure 1. Spherical isotropy jig showing probe, dipole and box filled with simulated brain liquid (see Ref [2], Section A.5.2.1)

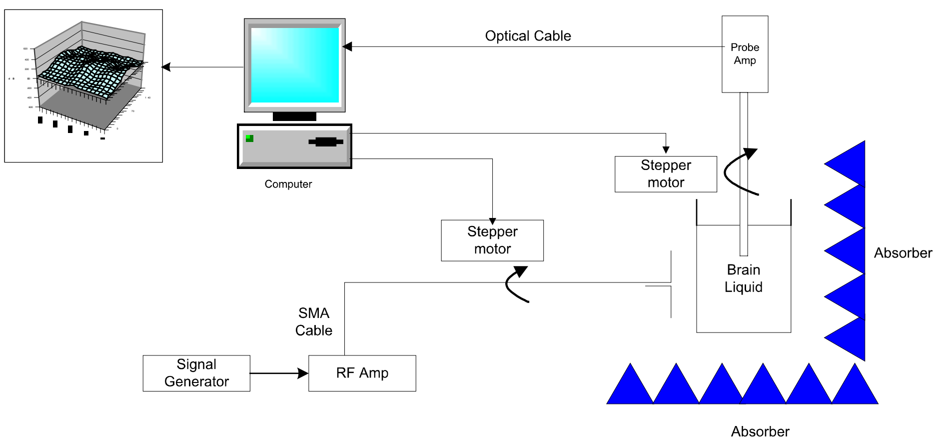

Figure 2. Schematic diagram of the test geometry used for isotropy determination

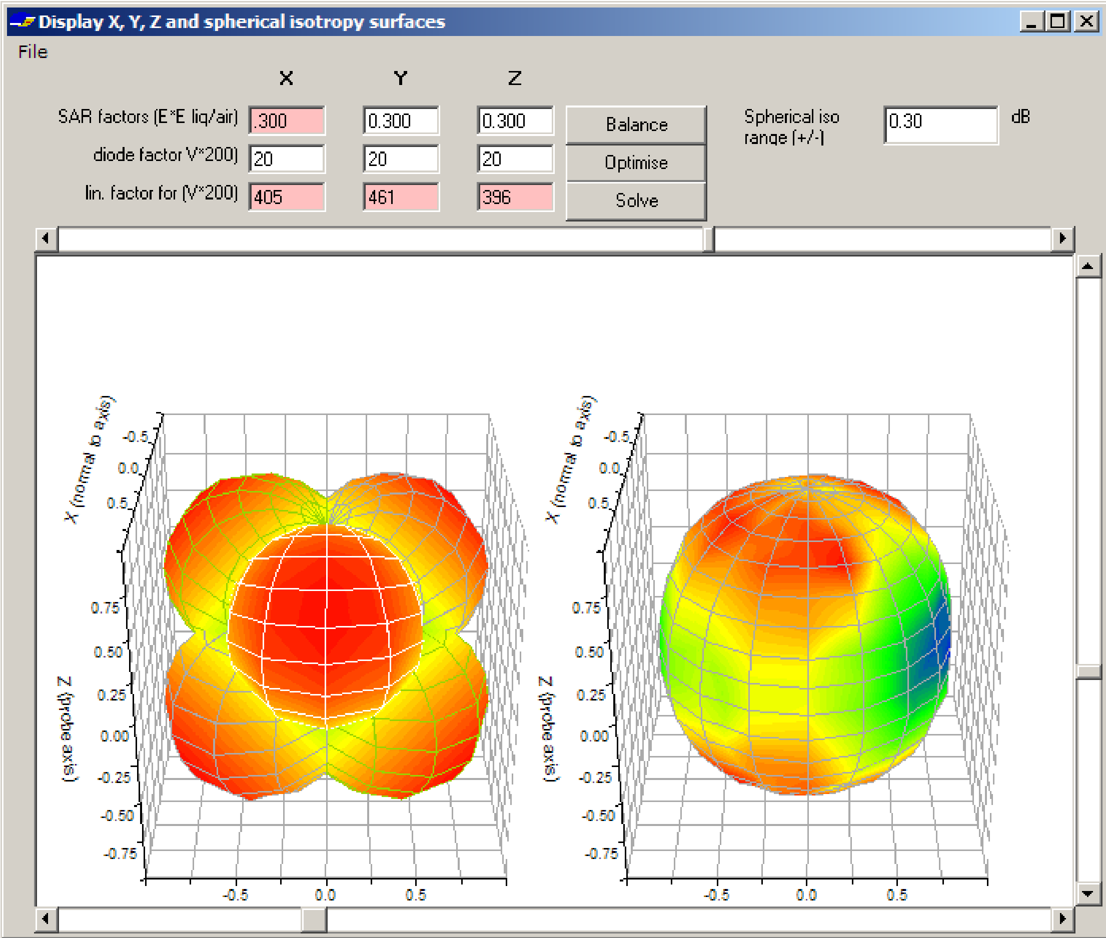

Figure 3. Graphical representation of the probe response to fields applied from each direction. The diagram on the left shows the individual response characteristics of each of the three channels and the diagram on the right shows the resulting probe sensitivity in each direction. The colour range in the figure images the lowest values as blue and the maximum values as red. For the probe S/N 0131, this range is (+/-) 0.30 dB. The probe is more sensitive to fields parallel to the axis and less sensitive to fields normal to the probe axis.

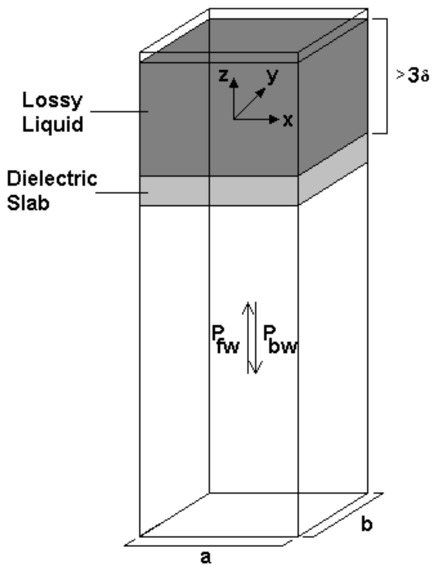

Figure 4. Geometry used for waveguide calibration (after Ref [2]. Section A.3.2.2)

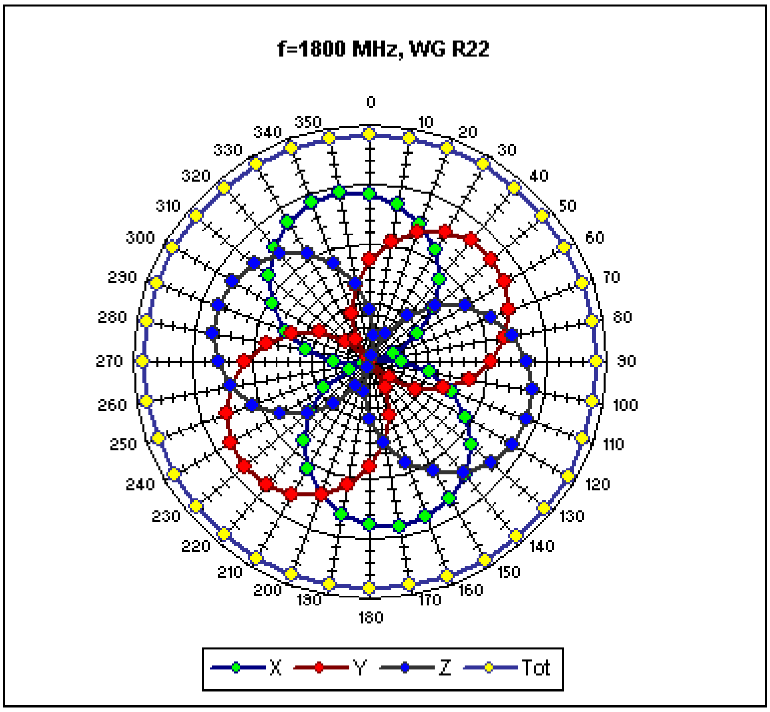

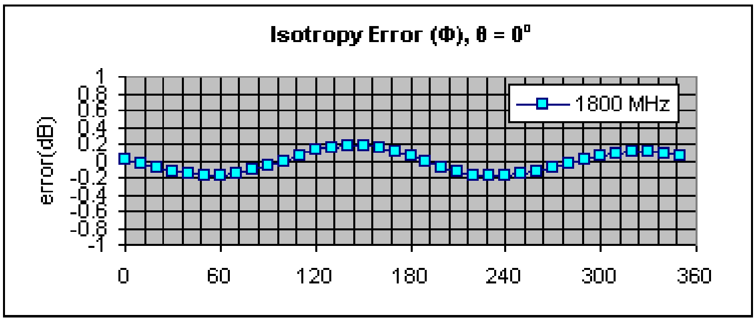

Figure 5. Example of the rotational isotropy of probe S/N 0131 obtained by rotating the probe in a liquid-filled waveguide at 1800 MHz. Similar distributions are obtained at the other test frequencies (1900 and 2450 MHz) both in brain liquids and body fluids (see summary table)

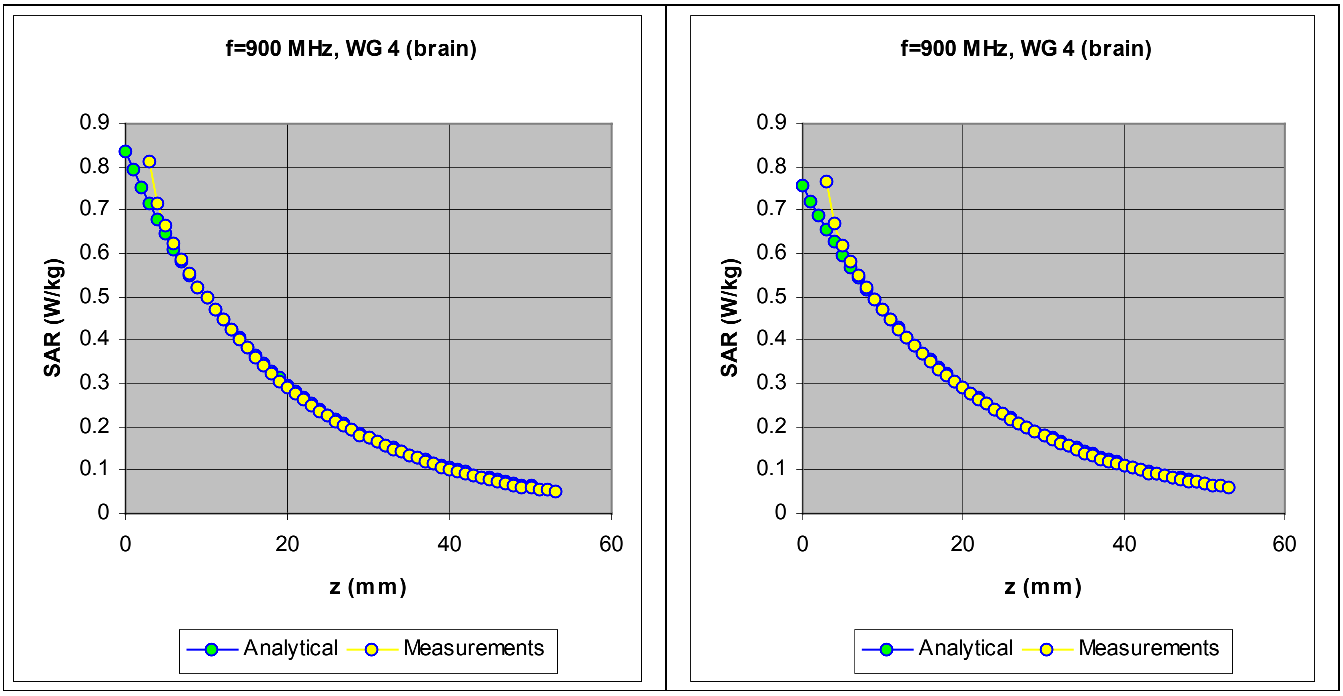

Figure 6. The measured SAR decay function along the centreline of the WG4 waveguide with conversion factors adjusted to fit to the theoretical function for the particular dimension, frequency, power and liquid properties employed.

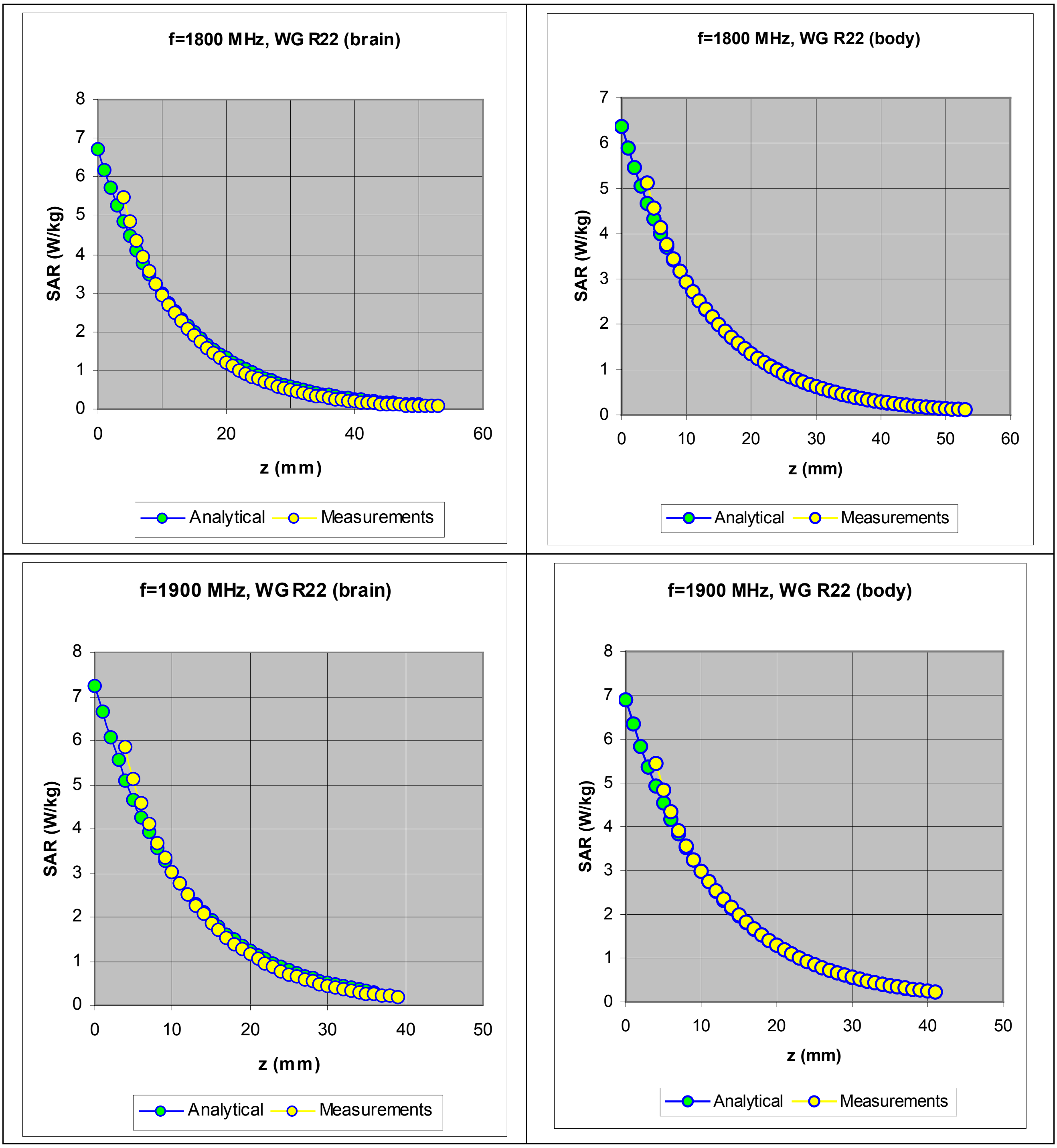

Figure 7. The measured SAR decay function along the centreline of the R22 waveguide with conversion factors adjusted to fit to the theoretical function for the particular dimension, frequency, power and liquid properties employed.

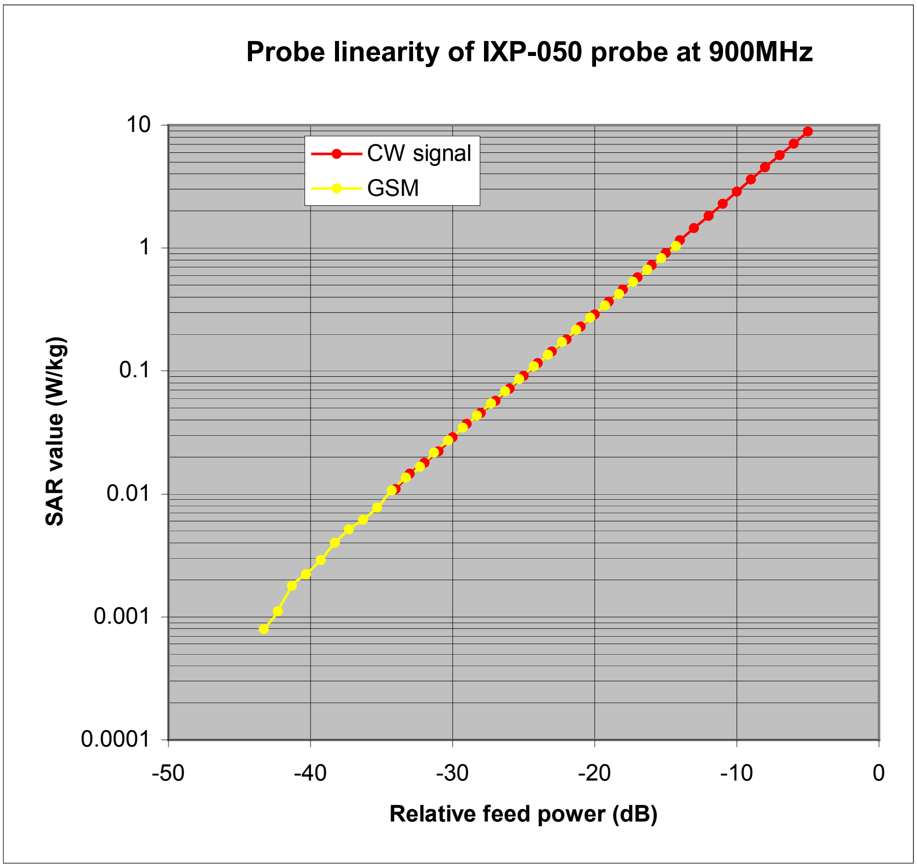

Figure 8. The GSM response of an IXP-050 probe at 900MHz.

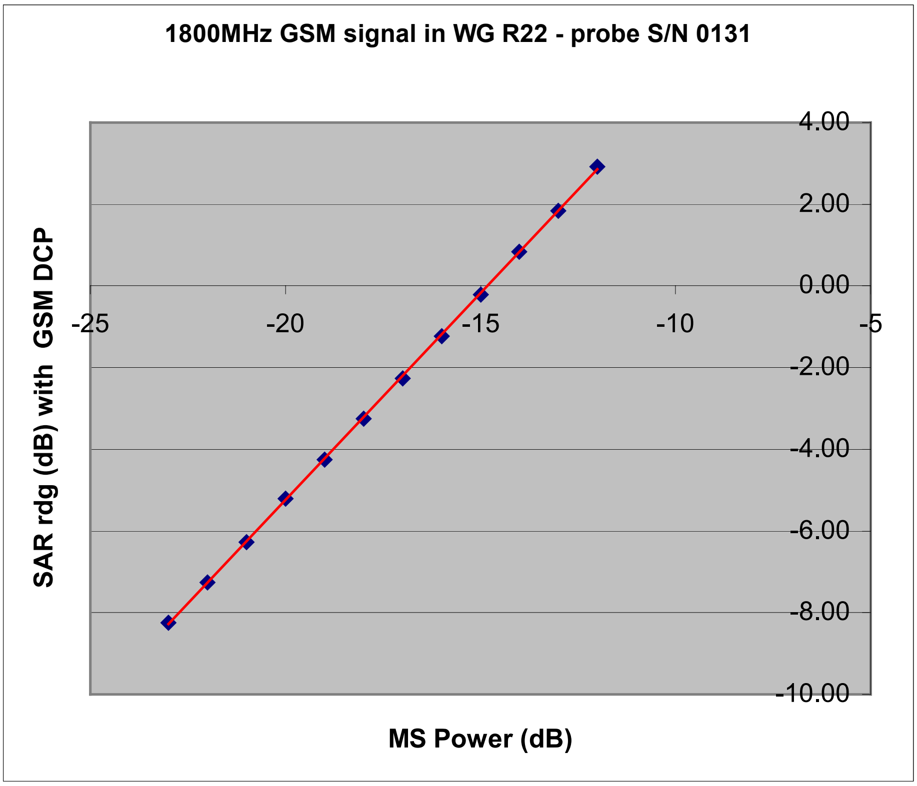

Figure 8a. The actual GSM response of IXP-050 probe S/N 0131 at 1800MHz

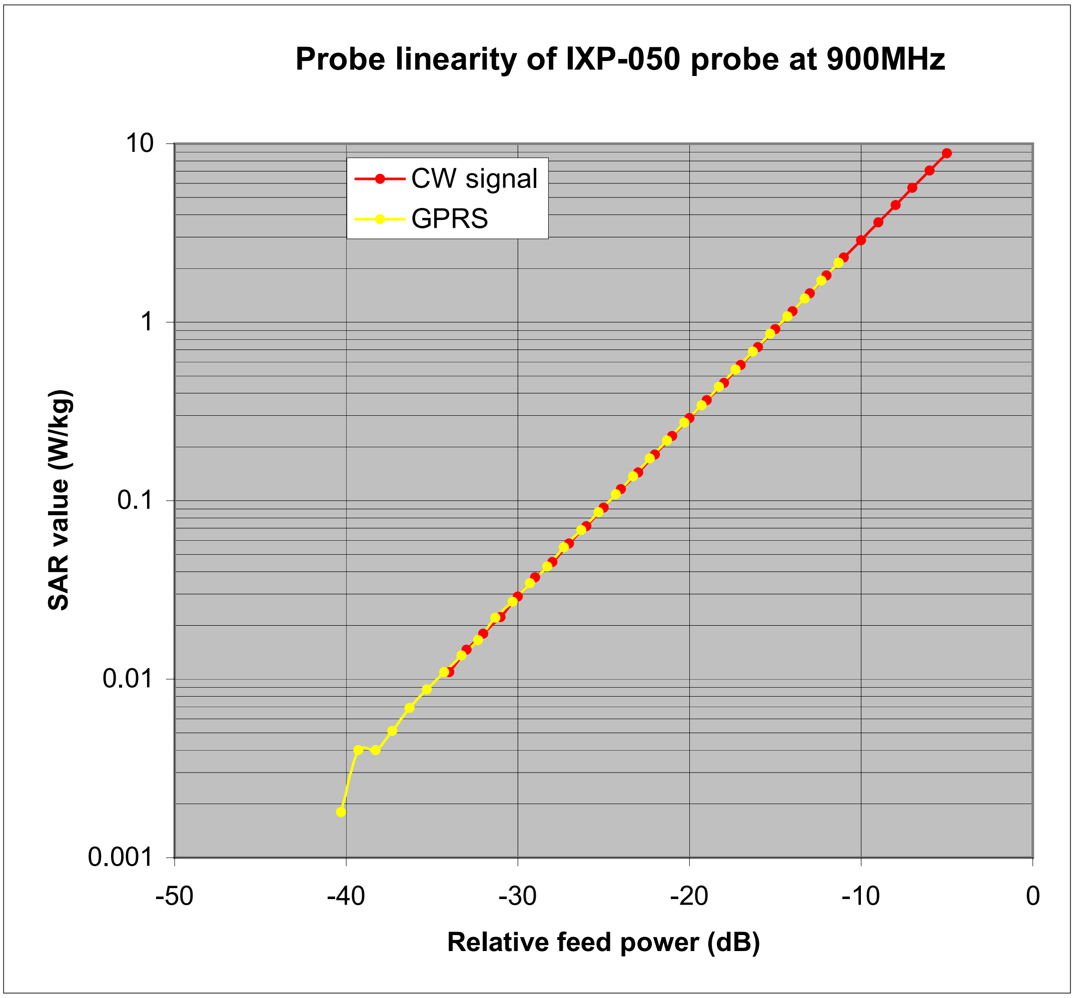

Figure 9. The GPRS response of an IXP-050 probe at 900MHz.

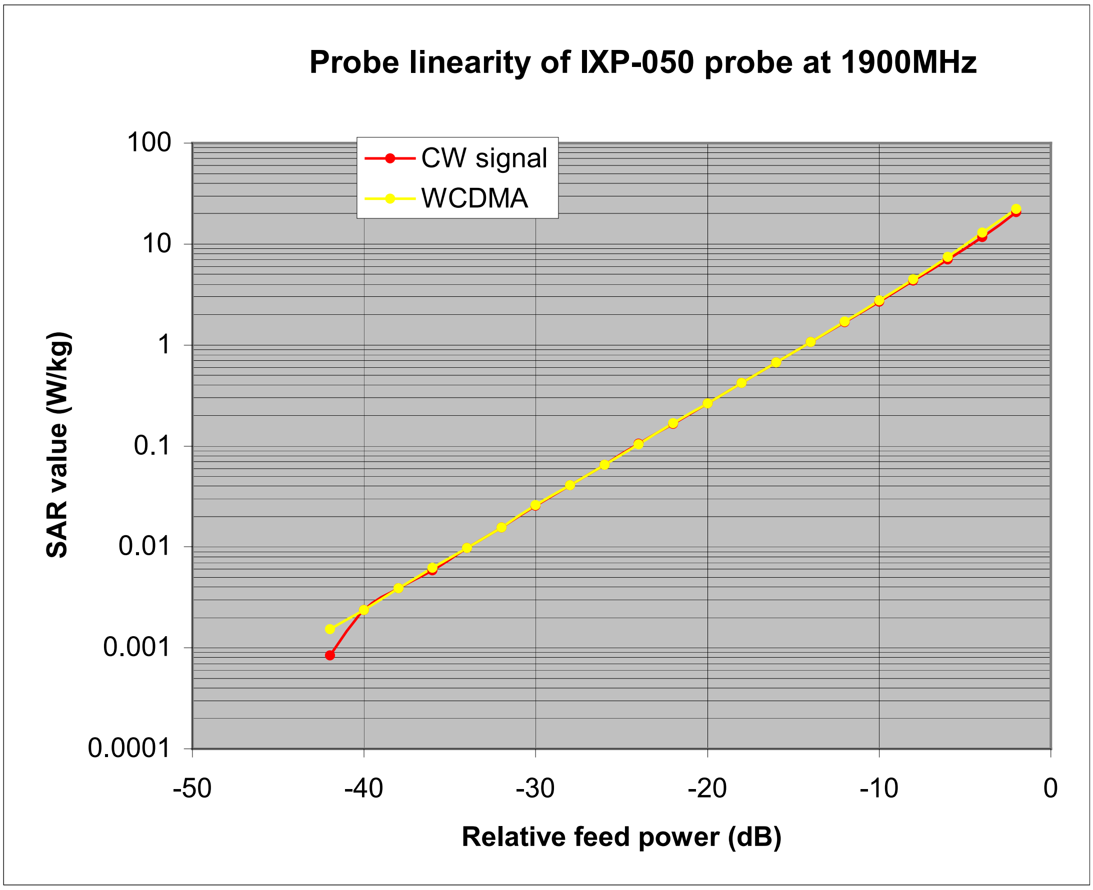

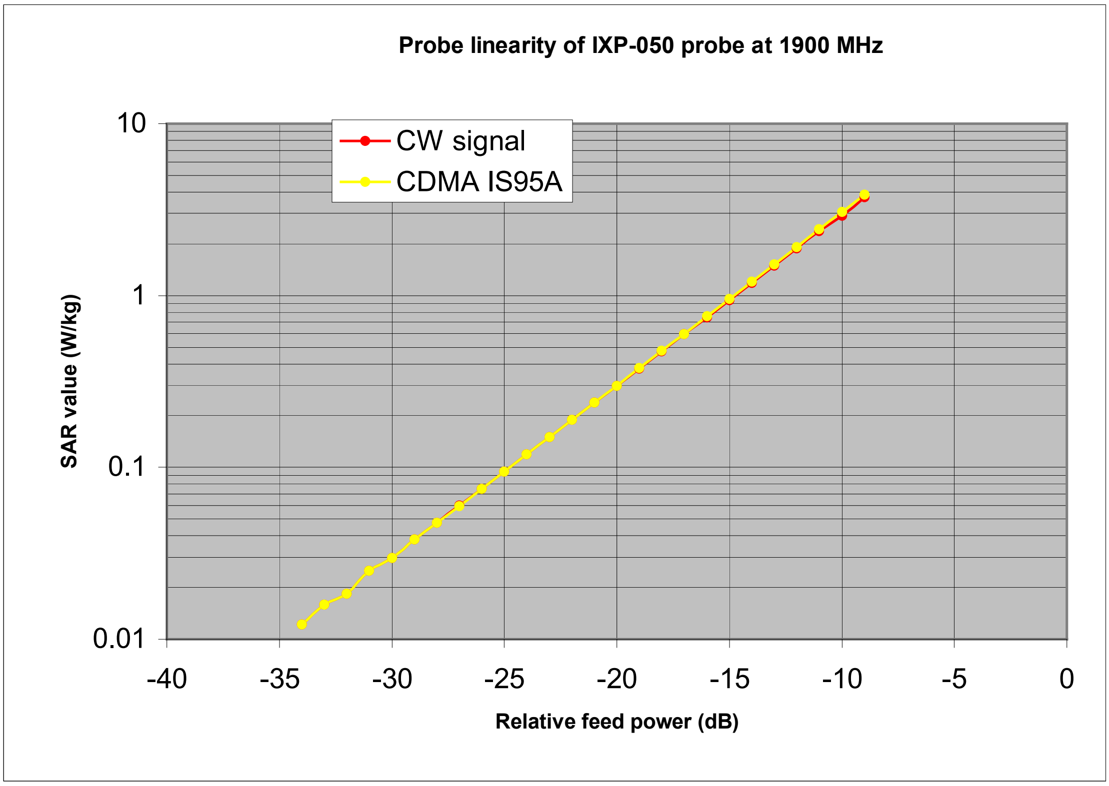

Figure 10. The CDMA response of an IXP-050 probe at 1900MHz.

Table indicating the dielectric parameters of the liquids used for calibrations at each frequency

Liquid used	Relative permittivity (measured)	Conductivity (S/m) (measured)
835 MHz BRAIN	43.18	0.935
835 MHz BODY	58.79	0.95
900 MHz BRAIN	42.47	0.998
900 MHz BODY	57.5	1.031
1800 MHz BRAIN	38.72	1.34
1800 MHz BODY	52.57	1.46
1900 MHz BRAIN	38.31	1.43
1900 MHz BODY	52.16	1.57
2450 MHz BRAIN	38.9	1.87
2450 MHz BODY	49.8	2.00
5200 MHz BRAIN	37.12	5.01
5200MHz BODY	54.36	5.55
5800 MHz BRAIN	35.41	5.79
5800 MHz BODY	52.62	6.53

COMPENSATING FOR THE FINITE SIZE OF SAR PROBES USED IN ELECTRIC-FIELD GRADIENTS

MI Manning, Indexsar Ltd.

Introduction

SAR probes with 3 diode-sensors in an orthogonal arrangement are designed to display an isotropic response when exposed to a uniform field. However, the probes are ordinarily used for measurements in non-uniform fields and isotropy is not assured when the field gradients are significant compared to the dimensions of the tip containing the three orthogonally-arranged dipole sensors.

It becomes increasingly important to assess the effects of field gradients on SAR probe readings when higher frequencies are being used. For Indexsar IXP-050 probes, which are of 5mm tip diameter, field gradient effects are minor at GSM frequencies, but are major above 5GHz. Smaller probes are less affected by field gradients and so probes, which are significantly less than 5mm diameter, would be better for applications above 5GHz.

In P1528, which covers frequencies up to 3GHz, Section 6.5.2 recommends that the probe axis should be oriented within 30 degrees to a line normal to the phantom surface to reduce probe boundary effects*:*

> *"If this angle is larger than 30 degrees and the closest point on the tip housing to the phantom surface is closer than a probe diameter, the boundary effect may become larger and polarization dependent. This additional uncertainty needs to be analyzed and taken into account, for which modified test procedures and additional uncertainty analyses not described in this recommended practice is required."*

This report describes theoretical and experimental studies to evaluate the issues associated with the use of probes at arbitrary angles to surfaces and field directions. Based upon these studies, the procedures and uncertainty analyses referred to in P1528 are addressed for the full range of probe presentation angles.

In addition, generalized procedures for correcting for the finite size of immersible SAR probes are developed. Use of these procedures enables application of schemes for virtual probe miniaturization (VPM) – allowing probes of a specific size to be used where physically-smaller probes would otherwise be required.

Given the typical dimensions of 3-channel SAR probes presently available, use of the VPM technique extends the satisfactory measurement range to higher frequencies.

Effect of sensor displacement from probe axis on spatial resolution

A measurement procedure is recommended in P1528 Section A.6.2 to investigate the effect of sensor displacement on spatial resolution. A sharp field minimum is introduced using parallel dipoles and the minimum is scanned using the probe. Such tests have been performed both at the side and the bottom of a box phantom using an Indexsar IXP-050 SAR probe. Details are given in Appendix 1. The results are similar at both the side and bottom of the box, but the response at the bottom of the box is smoothed out due to the displacements of the sensors in the field gradient direction. A sharper minimum is measured at the side of the box because the sensors are in the same plane as the field minimum. The results of this test demonstrate the potential for implementing procedures for compensating for sensor displacement.

Theory of probe response in a field gradient
When a SAR probe is exposed to any field gradient that is not aligned with the probe axis, each of the 3 individual sensors will be in regions of different field strength. However, the position recorded for the probe is the mid-point of all three sensors. Thus the sensors further away will read low and those closer to the source will read high. The situation is further complicated because the sensors are set at an angle to the probe axis (of +/- 54.7 degrees if the theoretical angle is employed) so that sensor sensitivity varies with the direction of the field polarization and that of the sensor dipole. In this report, this situation is analyzed first for the geometry used for isotropy testing (Fig A.2 in P1528 [1]), and subsequently for the generalized situation where the probe can have any angle to the local field gradient.

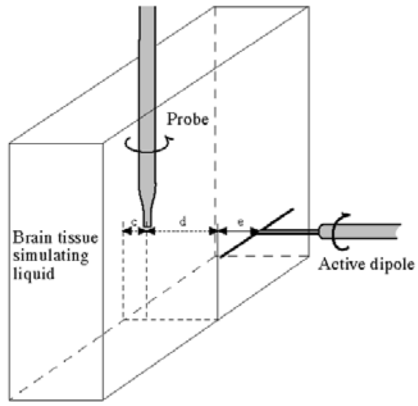

Figure 1: The test geometry illustrated in P1528 Figure A.2

The diagram below defines a coordinate framework and the angles of the source dipole and one of the sensor dipoles in the E-field probe.

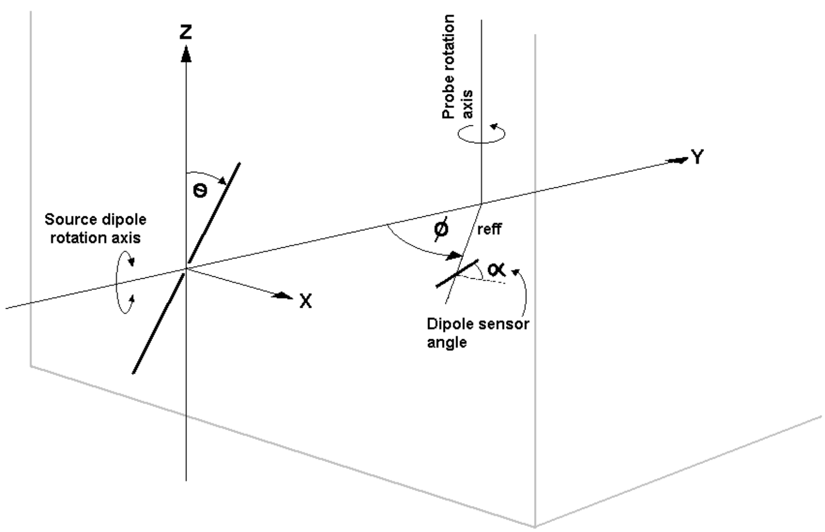

Figure 2: Coordinate system and angular reference points

In the Figure 2, θ is the angle of rotation of the source dipole with respect to the Z direction. Φ is the angle between the sensor location and the direction of the source. α is the sensor dipole angle from horizontal (this can be of either sign depending on the probe construction). r_{eff} is the effective sensor radius within the probe tip. Unit direction vectors for the source dipole and for the sensor dipole can be described as below

email: enquiries@indexsar.com http://www.indexsar.com
Oakfield House, Cudworth Lane, Newdigate, Surrey, RH5 5BG, UK.

source dipole unit vector: $X_d = \sin\theta$; $Y_d = 0$; $Z_d = \cos\theta$
sensor dipole unit vector: $X_s = \cos\Phi.\cos\alpha$; $Y_s = \sin\Phi$; $Z_s = \sin\alpha$

The sensor sensitivity is given by the cosine of the angle between them

$$\text{sensor sensitivity} = | X_d\, X_s + Y_d\, Y_s + Z_d\, Z_s |$$

$$= |(\sin\theta.\cos\Phi.\cos\alpha + \cos\theta.\sin\alpha)|$$

where the absolute value is taken since the sensor output is rectified. The magnitude of the local E-field also needs correction for position of the sensor down the field gradient

$$\text{distance correction} = e^{-r_{eff}.dr.\cos\Phi}$$

Where r_{eff} is the effective sensor radius, dr is the attenuation constant (= 1/ skin depth. See definitions in P1528 Section 3) and Φ is the sensor rotation from the source direction. For probe output which is (when linearised) proportional to E^2 or SAR,

$$\text{distance correction} = e^{-2.r_{eff}.dr.\cos\Phi}$$

The equations above allow us to calculate the variation of output of a diode sensor, U_{sensor}, with rotation angle

$$U_{sensor} = U_{centre}\ |(\sin\theta.\cos\Phi.\cos\alpha + \cos\theta.\sin\alpha)|\ e^{-2.r_{eff}.dr.\cos\Phi}$$

where U_{centre} is the value of the field at the centre of the probe tip

This equation can be used three times at angles 2π/3 apart to predict the isotropic response of a 3-channel probe in field gradients of different magnitude as shown in Figure 3.

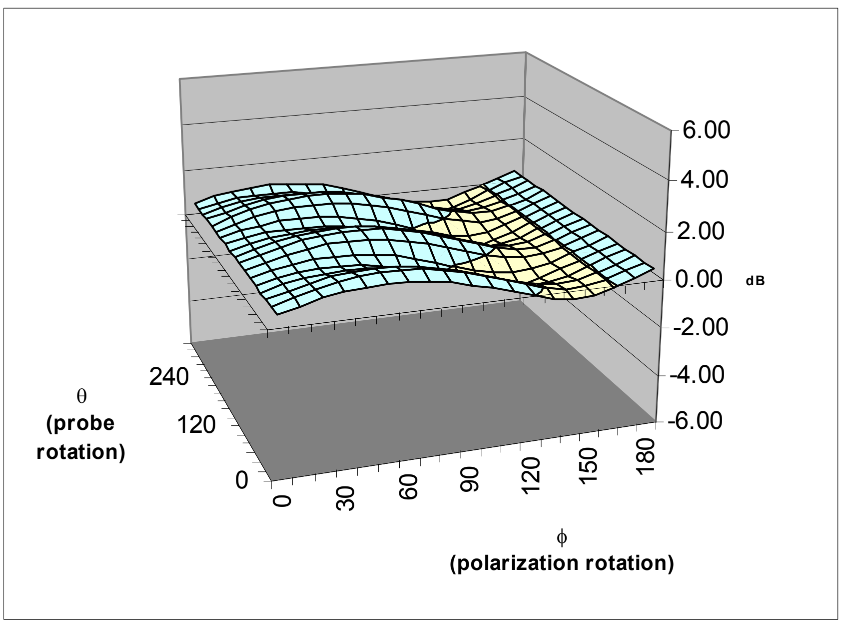

Figure 3: Predicted isotropic response of probe with an effective sensor radius of 1.25mm and a sensor angle of 35.3 degrees. The result shown is for a penetration depth of 9mm corresponding to 2450MHz box testing. The probe rotation is offset by 20 degrees to correspond with the measured data. The max. spherical isotropy range predicted is +/- 1.1227dB and the maximum rotational isotropy range is +/- 0.53 dB.

email: enquiries@indexsar.com http://www.indexsar.com
Oakfield House, Cudworth Lane, Newdigate, Surrey, RH5 5BG, UK.

The corrections require some knowledge of the direction and magnitude of the local field gradient. In this study, spot SAR measurements have been obtained and the frequency dependence of the magnitude of the field gradient can be deduced from related waveguide calibration measurements. However, the field decay rates in a waveguide (a unidirectional decay) are different from those in a box phantom, where field decays are omni-directional. In principle, 3D scanning measurements contain details of the field decay rate and of its direction, so an automated correction process can be implemented. Different levels of compensation procedure are considered below.

Uni-axial correction scheme for upright box phantom

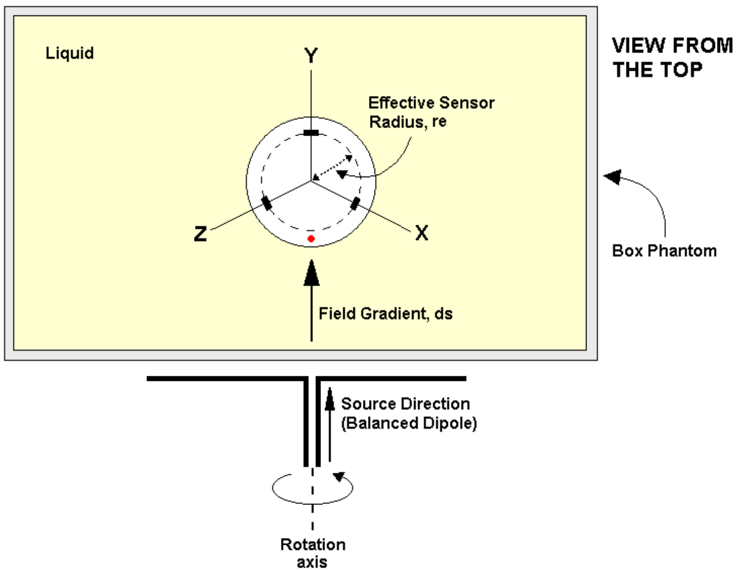

Figure 4: Illustration of the geometry for a uniaxial correction scheme.

With regard to Figure 4, which is looking down on a liquid-filled box phantom with a vertical probe, the probe outputs can be corrected by using the following equations:

$$X_c = X * EXP(-2\ r_{eff}\ dr\ COS(X_s))$$
$$Y_c = Y * EXP(-2\ r_{eff}\ dr\ COS(X_s + 2\pi/3))$$
$$Z_c = Z * EXP(-2\ r_{eff}\ dr\ COS(X_s + 4\pi/3))$$

where X_c is the corrected probe output, r_{eff} is the effective sensor radius, dr is the local decay rate as a factor per unit distance and X_s is the angle between the X sensor direction and the direction of source presentation (normal to the phantom).

Tri-axial correction scheme for generalized 3D data sets

Given a set of 3D gridded measurement data and details of the probe presentation angle at each position, the field gradients can be evaluated at each position and corrections for the offsets of each sensor in the gradient direction can be applied.

To develop the required formalism, assume that the gridded data and the probe positioning share the same Cartesian co-ordinate system. Assume that the probe axis is constrained to pass through the point X=0, Y=0, Z=0. Then, if the probe is at a position X, Y, Z, the probe presentation angle is obtained very simply from the position. For example, the inclination in the X-plane is ATAN(X/Z) and so forth for the other inclinations.

Each of the three sensors will have an offset from the nominal measurement location in the X, Y and Z directions. So there are 9 offsets in all:

For the x sensor:

X offset of x sensor = r_{eff} COS(X_s). COS(ATAN(X/Z))
Y offset of x sensor = r_{eff} SIN(X_s). COS(ATAN(Y/Z))
Z offset of x sensor = r_{eff} (SIN(X_s). SIN(ATAN(Y/Z)) + COS(Xs).SIN(ATAN(X/Z)))

Similarly for the other sensors but using Xs + 2π/3 or Xs + 4π/3 as appropriate.

The correction factors that need to be applied to each sensor measurement are obtained from the offsets by multiplying them by the local field gradients at each point. To obtain the local field gradients, the 3D gridded data are processed using a software algorithm to make a new array of the gradients at each point. A suitable algorithm is given in Appendix 2. Importantly, in this scheme, it is **not** necessary to have prior knowledge of the field gradients as they are evaluated from the measured data. Also, knowledge of the field polarization direction is not required.

The correction process involves replacing the measured 3D arrays of data with corrected arrays and then continuing with the remaining data post-processing stages

Experimental isotropy measurements in field-gradients 835MHz- 5.8GHz

In this study, a SAR probe has been maintained vertically in a rectangular liquid-filled phantom to which a dipole source has been applied from the side. The dipole source has been rotated through rotations from 0 to 180 degrees (angle between dipole arm and probe axis). It is important to realize that it is not sufficient to rotate the source through only 90 degrees as only half the probe anisotropy will be captured. In the measurement process, the probe is thus exposed laterally to the maximum available field gradient whilst the source polarization angle is varied. Dipoles dimensioned according to recommendations in P1528 (Annex G) have been used for frequencies from 835MHz through 2450MHz. The dipole used for 5200 and 5800 MHZ was improvised from a 2450MHz dipole and was not made according to recommendations that have subsequently appeared in a draft annex (Annex X) to P1528 (Table X.5).

The uncorrected measurements from 835MHz to 2450Mhz obtained agree very well with the theory presented above. For example, Figure 5 shows experimental measurement data for comparison with the analytically derived response shown in Figure 3.

email: enquiries@indexsar.com http://www.indexsar.com
Oakfield House, Cudworth Lane, Newdigate, Surrey, RH5 5BG, UK.

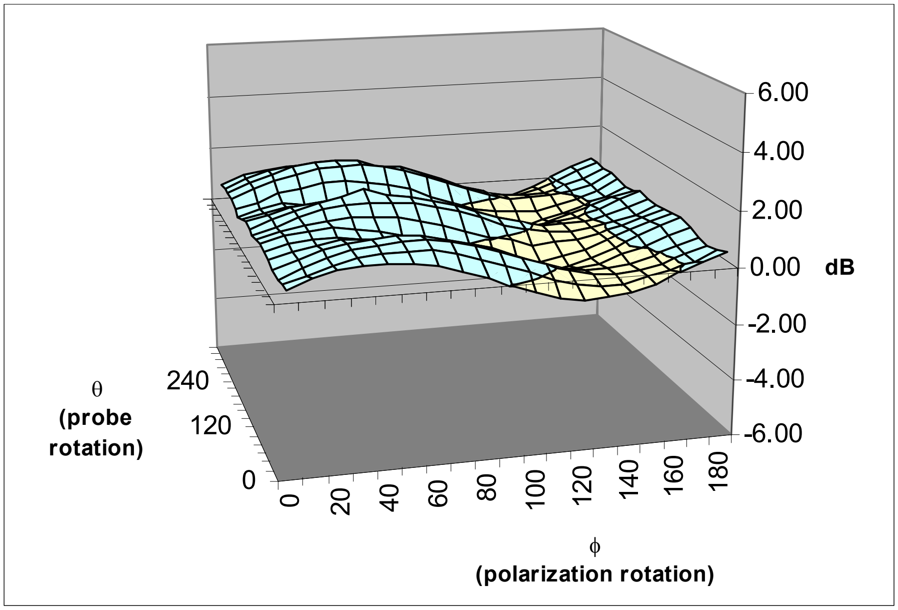

Figure 5: Measured isotropic response of an IXP-050 probe with tip diameter of 5 mm at 2450MHz. The probe rotation started with the X sensor at 20 degrees rotation to the source. The max. spherical isotropy range measured was +/- 1.136dB and the maximum rotational isotropy range was +/- 0.79 dB.

Measurement results were obtained at frequencies between 835MHz and 58000MHz and are shown graphically in Figures 6 – 9 below and summarized in Table 1. Corrections have been applied using the uni-axial procedure developed from the analytical equations. For these corrections, an effective sensor radius of 1.25mm was used in all cases and the penetration depth in the box for optimum corrections is as shown in brackets in Table 1 column 5. Box penetration depths would be expected to be somewhat less than for a uni-directionally dispersing wave in a waveguide.

email: enquiries@indexsar.com http://www.indexsar.com
Oakfield House, Cudworth Lane, Newdigate, Surrey, RH5 5BG, UK.

Table 1: Results - Spherical isotropy range versus frequency

Frequency (MHz)	Max. anisotropy in field gradient – uncorrected (+/- dB)	Max. anisotropy corrected for field gradient (+/- dB)	Rotational isotropy in field gradient (+/- dB)	Penetration depth (E) from waveguide decay meas. (and in box) (mm)	IXP-050 Probe S/N
835	0.464	0.368	0.22/0.14	49.0 (36)	0084
900	0.542	0.330	0.28/0.17	34.9 (28)	0084
1800	0.884	0.556	0.57/0.31	24.0 (11)	0084
2000	1.323	0.705	0.86/0.32	20.0 (10)	0084
2450	1.136	0.789	0.79/0.44	18.0 (9)	0084
5250	3.111	1.023	1.85/0.83	5.73 (4)	0125
5800	3.293	1.014	2.07/0.94	5.25 (4)	0125

Table 2: Dielectric properties for the liquids used in the box phantom tests at each frequency

Frequency (MHz)	Relative permittivity	Conductivity (S/m)
835	42.9	.89
900	42.5	.97
1800	39.50	1.74
1900	38.77	1.86
2450	35.10	2.45
5250	43.60	6.3
5700	40.09	6.6

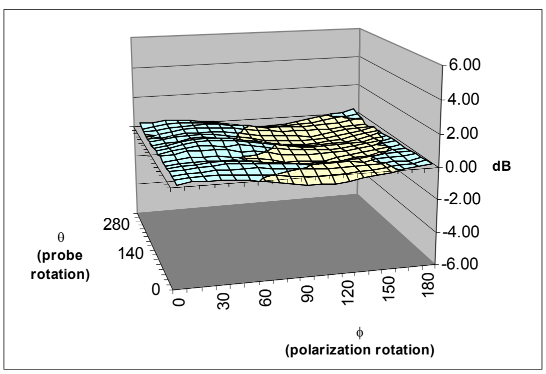

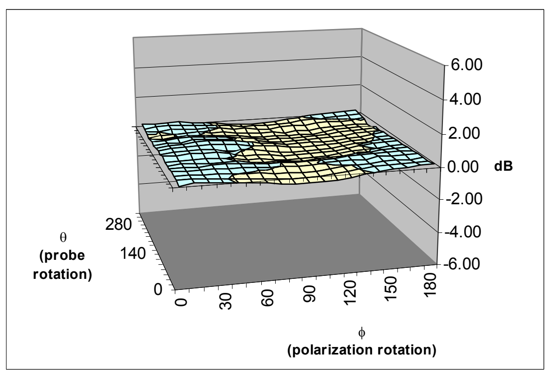

Figure 6: Probe isotropy at 900MHz with probe oriented at 90 degrees to field gradient direction. At left, uncorrected readings. At right, corrected for sensor displacement.

email: enquiries@indexsar.com   http://www.indexsar.com
Oakfield House, Cudworth Lane, Newdigate, Surrey, RH5 5BG, UK.

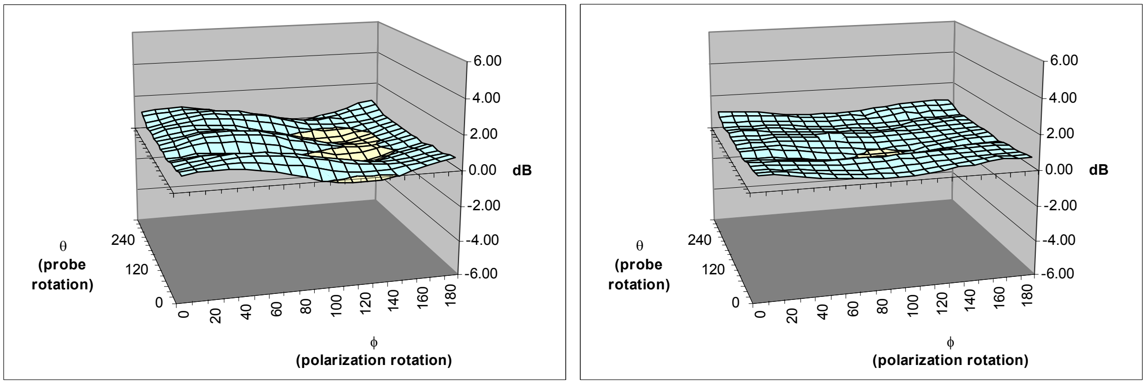

Figure 7: Probe isotropy at 1800MHz with probe oriented at 90 degrees to field gradient direction. At left, uncorrected readings. At right, corrected for sensor displacement.

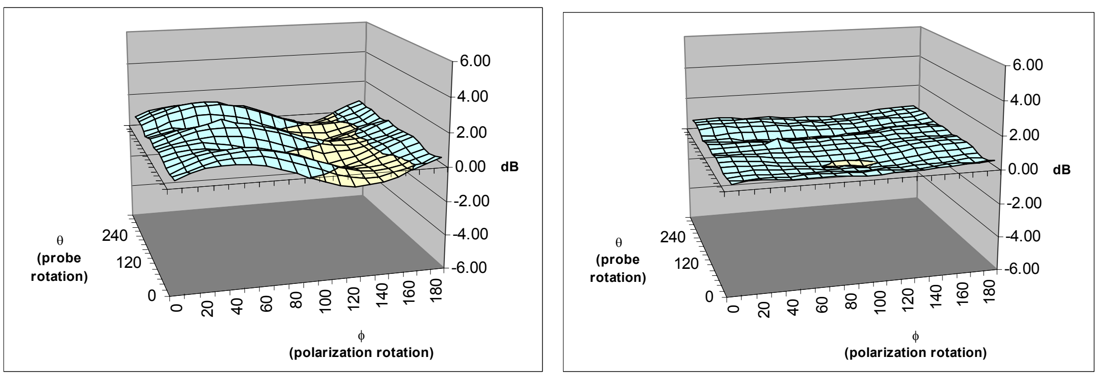

Figure 8: Probe isotropy at 2450MHz with probe oriented at 90 degrees to field gradient direction. At left, uncorrected readings. At right, corrected for sensor displacement.

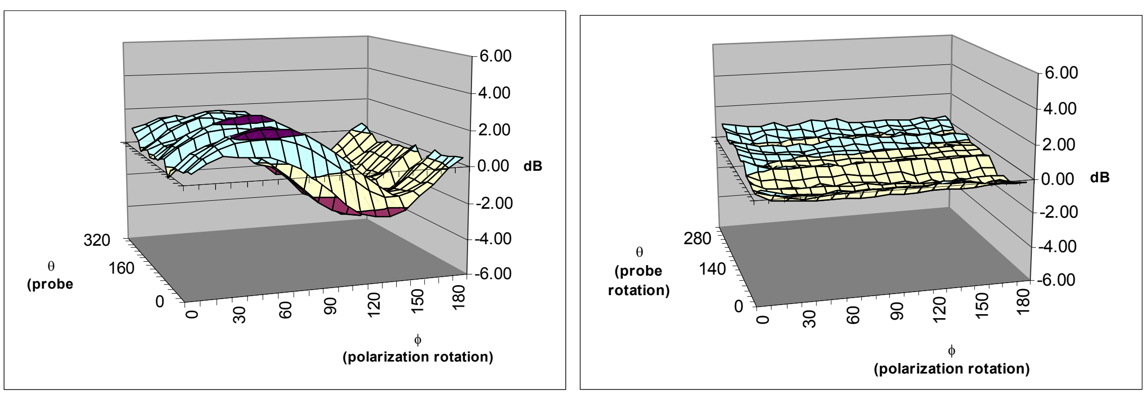

Figure 9: Probe isotropy at 5250MHz with probe oriented at 90 degrees to field gradient direction. At left, uncorrected readings. At right, corrected for sensor displacement. ***Note:*** *dipole used was not dimensioned according to new draft Annex X recommendation for P1528. Additionally, deficiencies in the bearing used to rotate the probe during testing are thought to be the reason for much of the residual variability in the right-hand plot.*

3D scheme for boundary effects correction

The framework introduced above for sensor offsets corrections provides a good foundation for the implementation of an omni-directional boundary effects correction scheme. The starting point for this is the magnitude of the boundary effect error that is deduced from waveguide probe calibration measurements. A typical uncorrected waveguide centerline profile fitted to analytical expectations without correction is shown in Figure 10.

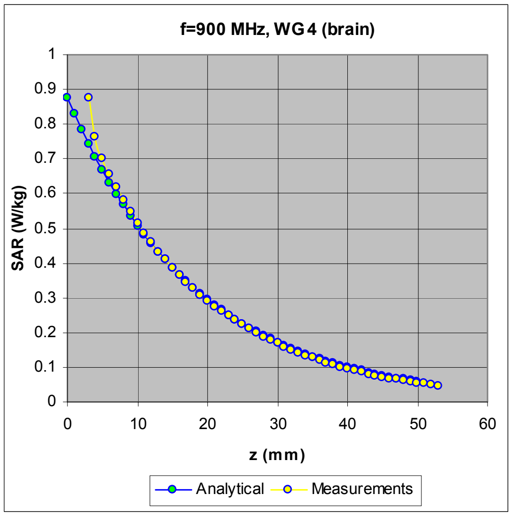

Figure 10: 900MHz waveguide measurement without boundary correction

The following correction implements a satisfactory correction scheme for the waveguide measurements as illustrated in Figure 11, where the correction equation has been applied

$$S_{corr} = S * (1\text{-alpha*EXP}(-x/d))$$

where S_{corr} is the SAR measurement corrected for the boundary effect, S is the uncorrected SAR reading, alpha is the correction term for the surface value overestimation and d is the influence depth over which the effect arises. x is the sensor depth from the phantom surface within the lossy liquid.

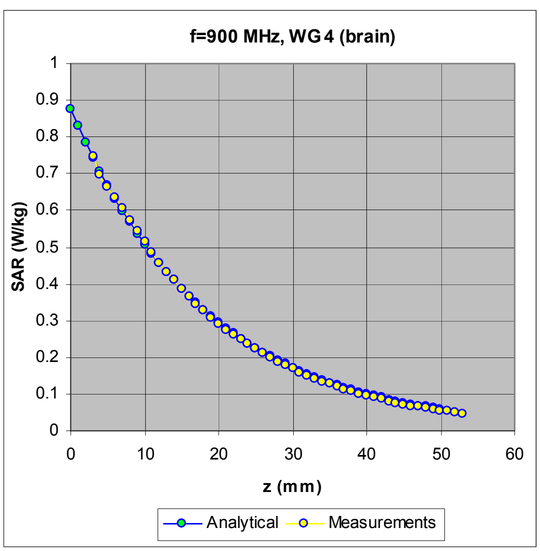

Figure 11: 900MHz waveguide measurement with boundary correction

email: enquiries@indexsar.com http://www.indexsar.com
Oakfield House, Cudworth Lane, Newdigate, Surrey, RH5 5BG, UK.

This correction is basically required because of a geometrically-related influence as the probe approaches the surface and this is supported by measurements, which show a relative insensitivity of the correction factors to frequency or liquid properties. For the Indexsar probes tested, values of alpha=0.65 and d=2mm provide most of the correction required at all frequencies tested and for brain and body liquids.

In the SAR measurement situation with the VPM correction scheme implemented, the probe orientation with respect to the co-ordinate system used for scanning is known and the position and orientation of the phantom surface are also known. The probe orientation has already been used at each point to compute the adjusted sensor positions in 3D and so it is straightforward to apply a separate boundary proximity correction for each sensor based on this information.

There are issues associated with this convenient, procedural approach. Boundary corrections may be thought to be less necessary when the curved side of a probe is brought against a phantom surface compared to the situation of end-on presentation as in a waveguide when all the lossy-liquid is squeezed out at the point of contact. Also, waveguide-determined correction factors are not necessarily applicable to thin-walled phantoms because the thickness and relative permittivity of the liquid barrier are radically different in each case. So, boundary correction schemes probably require a fair amount of further study. Separate corrections for each of the three sensors would seem to be a necessary part of a general correction algorithm and have been implemented in the latest SARA2 software. The success or completeness of this approach will only be finally judged after further experience and testing.

Effects of the corrections on measured SAR profiles

To evaluate the magnitude of the VPM and boundary corrections, the corrections have been applied to scans against a balanced 1800MHz dipole placed at the vertical side of a 2mm wall box phantom. The dipole was oriented vertically and also at 45 degrees to the vertical leaning both to the left and to the right. With the dipole to the left, it is approximately parallel to the nearest sensor of the probe tip, whilst when to the right, it approximately normal to the closest dipole. These therefore represent extremes of the polarization influences. In Figures 12 to 14, the effects of the corrections applied to a central profile from the 3D scans are shown. The first correction applied is the full 3D VPM scheme, where the field gradients are deduced from the 3D measured data. The boundary corrections are applied separately to each sensor based on the scheme and factors referred to above.

email: enquiries@indexsar.com http://www.indexsar.com
Oakfield House, Cudworth Lane, Newdigate, Surrey, RH5 5BG, UK.

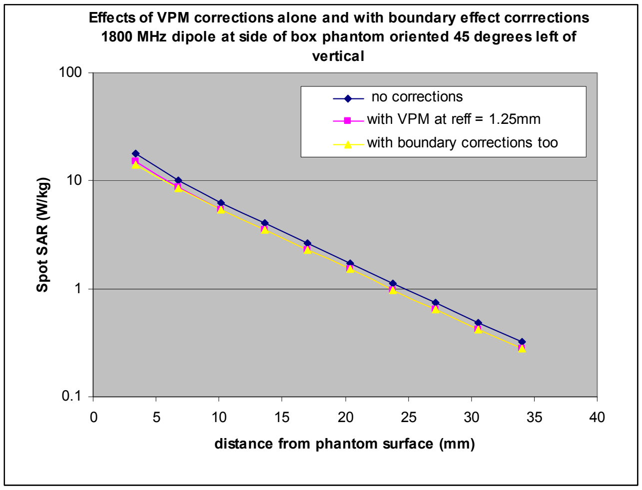

Figure 12: Source dipole oriented approximately parallel to nearest probe sensor

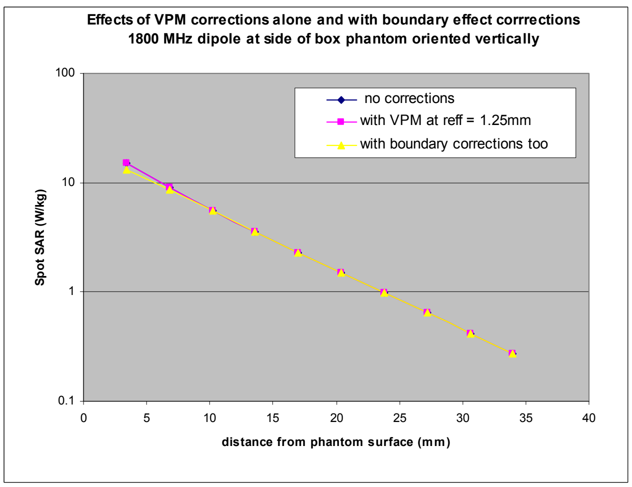

Figure 13: Source dipole oriented vertically (the uncorrected and VPM-corrected lines are essentially co-incident)

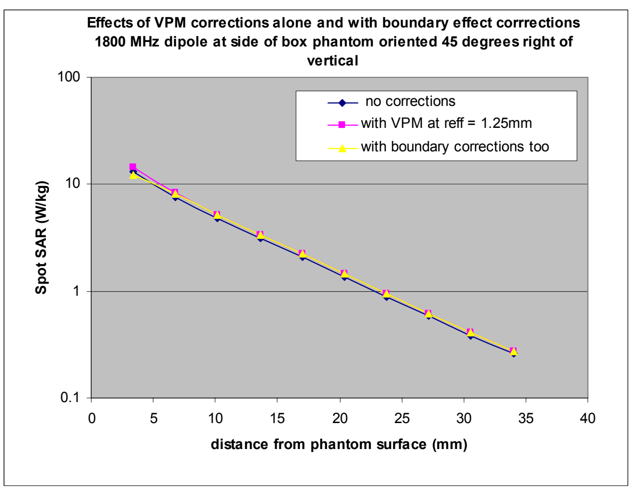

Figure 14: Source dipole oriented approximately normal to nearest probe sensor

Discussion
The analysis presented here shows that even for a SAR probe with ‘perfect’ geometry and construction, spherical isotropy is unavoidable. When the E-field penetration depth and the tip diameter are comparable, the isotropy range is around +/- 3dB.

The explanation for the analytically-derived isotropy response of probes in field gradients is that the sensor closest to the source is preferentially disposed to overestimating the contribution of fields polarized parallel to the direction of that sensor compared to the contribution of the sensors further away, which have different orientations compared to the applied field polarization. Conversely, the closest sensor is preferentially disposed to underestimating the contribution of fields perpendicular to the direction of that sensor compared to the contribution of the sensors further away. This behaviour introduces a predictable anisotropic response for field orientations that do not align with the probe axis or the plane of its normal. For field polarization directions either normal or perpendicular to the probe axis, the probes retain good isotropy even in field gradients.

The correction procedure proposed in this Report adjusts the values of the field measured by each sensor to make allowance for its actual effective displacement in the field gradient direction compared to where the middle of the probe sensor array is assumed to be. The correction procedure does not require any knowledge of the field polarization direction – just of the field gradient direction.

This process requires that the orientation of the probe and the angular positions of the three sensors within it are known in comparison with the direction of the field gradient. Given this, the displacement of each sensor from the central position can be allowed for if the field gradient is known. The field gradients can be deduced from measured data in a 3D array.

It has been found in this study that the effective displacement of each sensor from the middle position is not given by its physical radius, but is approximately half of the tip radius for the probes investigated. With this established, the corrections for sensor position are simply related to the effective geometrical displacement of each sensor in the direction of the maximum field gradient and to the magnitude of this maximum field gradient.

At 2450MHz the highest frequency (and worst-case) considered within the P1528 range, different schemes for controlling field gradient effects have been compared based on the results obtained as in Table 3.

Table 3: Comparing different schemes for managing SAR probe anisotropy in field gradients at 2450MHz

Reduction scheme	Isotropy range (+/- dB)	Percentage error (+/- %)
None (all angles allowed)	1.136	30
+/- 30 degree constraint	0.844	21
Uni-axial VPM scheme (all angles allowed)	0.789	20
Uni-axial scheme and +/- 40 degree constraint	0.500	12

The implication for upright SAM phantom measurements is that the probe may read low or high at high frequency depending on the source presentation angle. This might most-usually lead to an underestimate at the LH ear (DUT with dipole antenna) but similar overestimate at the RH ear. For the Indexsar probe construction and an upright head, the dipole sensor closest to the surface is in approximate alignment with a handset centerline at the RH ear and approximately normal to it at the LH ear. These effects are small at GSM frequencies, but need correction for higher frequencies – especially over 5GHz.

email: enquiries@indexsar.com http://www.indexsar.com
Oakfield House, Cudworth Lane, Newdigate, Surrey, RH5 5BG, UK.

The VPM correction scheme introduced in this document allows for this and offers comparable or better uncertainty reductions compared to the +/-30 degree constraint proposed in P1528 but without requiring any constraint on probe presentation angles. If used in combination with an angle constraint (see last line of Table 3), much lower uncertainties should be achievable. This correction will certainly need to be applied for any tests >5GHz even with the probe normal but, in any case, lower uncertainties will be achieved by performing measurements at the bottom of a phantom box (for field polarization directions not aligned with the probe axis or its normal).

The box-phantom test geometry used here for isotropy assessment in a field gradient is particularly relevant for upright phantom geometries and provides a realistic assessment of achievable SAR probe isotropy in a field gradient, which is a much more onerous test that that of assessing the isotropy in a uniform field or of reporting solely the rotational isotropy where the direction of field decay is conveniently arranged to align with the probe axis direction (this orientation, widely used for probe calibration, is a unique configuration whereby all three sensors are equally far removed from the source. But any measured SAR distribution will contain field gradients of arbitrary direction and probe anisotropy in response to changing field directions must be considered. This requirement is equally true for probes held perpendicular to the phantom surface as for any other probe presentation geometry (i.e. it is nothing particularly specific to the upright phantom geometry but affects flat-bath measurements as well).

It has been shown that that the isotropy of an immersed SAR E-field probe having traditionally-arranged sensors (on a triangular core) in a field gradient is the same as that in a uniform field when the applied field polarization direction aligns with either the probe axis direction or is normal to the probe axis direction.

Indexsar have frequently reported the equivalence of parallel and normal field measurements. Results have been presented in several Indexsar Reports [2, 3, 4]. These studies compared results obtained from performing scans with the source both at the side of a box phantom (upright geometry) and at the bottom of a box (horizontal geometry). Results from both measurement configurations have been shown to be equivalent. At the side of the box, both horizontal and vertical field polarizations were compared and found to give equivalent results.

The conclusions of these previous studies [2, 3, 4] remain. This new study expands the previous assessments to other field polarisation angles that do not necessarily align with the probe axis or the plane of its normal – a situation that applies in normal device measurement.

With Indexsar IXP-050 probes, the tip casing is of 5mm diameter, but the dipole sensors are interleaved, with the objective of getting the physical centers of the diode-loaded sensors closer together. This study suggests that interleaving the sensors is reducing the effective size of the probe.

The use of the VPM technique described substantially reduces the effective size of the SAR probes over the P1528 frequency range. At frequencies between 5-6GHz, the surface SAR value decays to 1/e of its value in a depth of only 2-3mm. Whilst VPM corrections can reduce the (otherwise large) isotropy range of 5mm probes, the sensor-tip separation distance is such that substantial measurement extrapolations are required for volume averaging. It is anticipated that both smaller probes and the application of VPM would be needed to reduce the isotropy range.

Conclusions

1) The recommendation in P1528 that spherical isotropy range should be determined using angles of incidence from 0 to 90 degrees could potentially lead to only half of the actual spherical isotropy range being collected in the measurements. The theory above shows that it is necessary to perform spherical isotropy measurements over a full 180 degree range (as in Indexsar probe calibrations and as in the tests reported).

email: enquiries@indexsar.com http://www.indexsar.com
Oakfield House, Cudworth Lane, Newdigate, Surrey, RH5 5BG, UK.

2) This study indicates that the effective sensor radius of the orthogonally-arranged sensors in a SAR probe is a characteristic of such probes, which would merit routine determination and reporting.

3) P1528 recommends that probe axis is oriented within +/-30 degrees of the normal to the phantom surface. This requirement could be (and ought to be) more accurately expressed as that the probe axis should be oriented within +/- 30 degrees of the local field gradient. Obviously, the field gradient direction varies with position in any 3D or zoom scan and is not always aligned with the local normal to the phantom surface.

4) The virtual probe miniaturization (VPM) scheme is proposed as an improved technique (compared to +/- 30 degree angle limitations in P1528) that does not require constraint of the probe presentation angle to the local field gradient direction.

5) Existing P1528 recommendations make inadequate distinction between boundary effects and field gradient effects. The field gradient effects, which are dominant, are not related to proximity to the phantom surface, but extend throughout the full measurement range used in SAR testing. Boundary effects will not be fully understood without appreciating field gradient effects.

6) The computational framework needed for corrections of field gradient effects also provide a platform for the correction of boundary effects when the boundary is in an arbitrary direction from the probe axis.

7) The correction procedures proposed can be applied for all systems, where 3-channel SAR probes are used for SAR measurements in 3D.

(VPM corrections as well as an omni-directional probe boundary effect correction scheme have been included in the processing algorithms used by the latest SARA2 software).

Implications for P1528 uncertainty assessment

Table 1 indicates that application of a VPM scheme (as described in this document) is at least as effective in managing probe isotropy uncertainties as is the +/- 30 degree probe presentation angle restriction (to the local phantom surface normal) suggested in P1528. Importantly, this new scheme dispenses with the need for any angle restriction. So, application of a VPM scheme is preferable to a limitation on probe presentation angle. Inspection of figures 3-9 shows that the gradient of probe anisotropy with probe orientation is actually a maximum at the angle of probe normal incidence, so it is not a good idea to rely upon a +/- 30 degrees presentation criterion. Without correction, probe anisotropy is still significant in field gradients to an extent dependent upon frequency. The errors involved for +/- 30 degrees are simple to determine from the theory presented. Application of the VPM scheme will also help manage (the still significant) errors associated with probes presented within +/- 30 degrees of the local surface normal.

A source of uncertainty in the application of this scheme relates to how well the orientation of the sensors within the probe casing are known in relation to the scanning coordinate system. The sensor angular positions need to be known in relation to a reference mark on the probe casing. This can be established during probe calibration using, for example, an arrangement such as that shown in Figure 1. The variations caused by errors in lining up the reference mark can be determined by applying intentional offsets and examining the variations in the VPM-corrected SAR results.

email: enquiries@indexsar.com http://www.indexsar.com
Oakfield House, Cudworth Lane, Newdigate, Surrey, RH5 5BG, UK.

References

[1] P1528 Recommended practice for determining the peak spatial-average absorption rate (SAR) in the human head from wireless communications devices: Measurement techniques. IEEE Std 1528.

[2] IXS209 Error assessment for probe / interface proximity effects for an upright phantom geometry, Indexsar Report, April 2002.

[3] IXS214 Error assessment for probe / interface proximity effects at 1800MHz, Indexsar Report, September 2002.

[4] IXS215 SARA2 validation testing with CDMA-modulated signals at bottom and side of phantom at 1900MHz, October 2002.

Appendix 1: Effect of sensor displacement from probe axis on spatial resolution
A measurement procedure is recommended in P1528 Section A.6.2 to investigate the effect of sensor displacement on spatial resolution. A sharp field minimum is introduced using parallel and opposed dipoles and the minimum is scanned using the probe. Tests have been performed both at the side and the bottom of a box phantom an Indexsar IXP-050 SAR probe. An Indexsar 1.3mm probe was also used. The recommended configuration is reproduced in Figure A1.1.

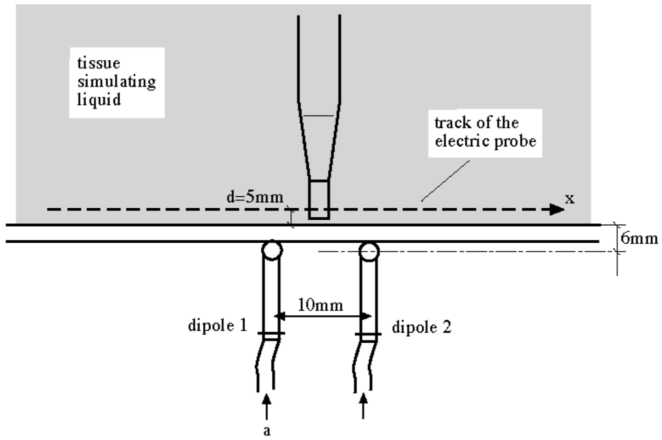

Figure A1.1: Setup used for investigating the behavior of dosimetric probes in normal and strong gradient fields [1]. The dipoles are parallel to each other and orthogonal to the page

This test set-up has been implemented for testing both at the bottom of a box phantom and at the side. The set-up at the side is illustrated in Figure A1.2.

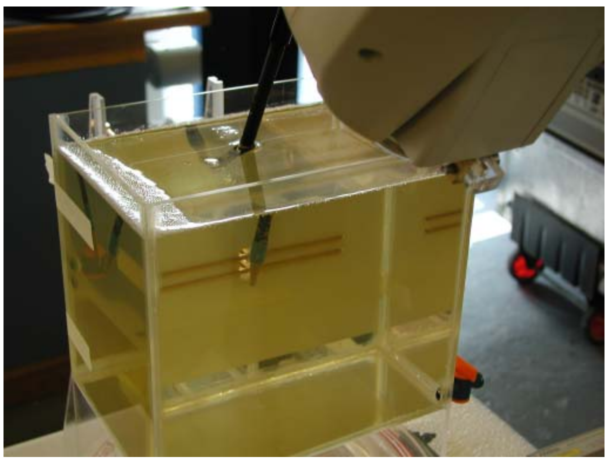

Figure A1.2: Implementation of the test arrangement at the side of a box phantom using 900MHz dipoles

The results obtained by scanning the 1.3mm and 5mm probes across the field minimum between the dipoles are shown in Figure A1.3. A sharper dip is registered at the side of the box for the 5mm probe because the sensor displacements from the plane of the minimum are less in this geometry at the mid-point between the dipoles.

email: enquiries@indexsar.com http://www.indexsar.com
Oakfield House, Cudworth Lane, Newdigate, Surrey, RH5 5BG, UK.

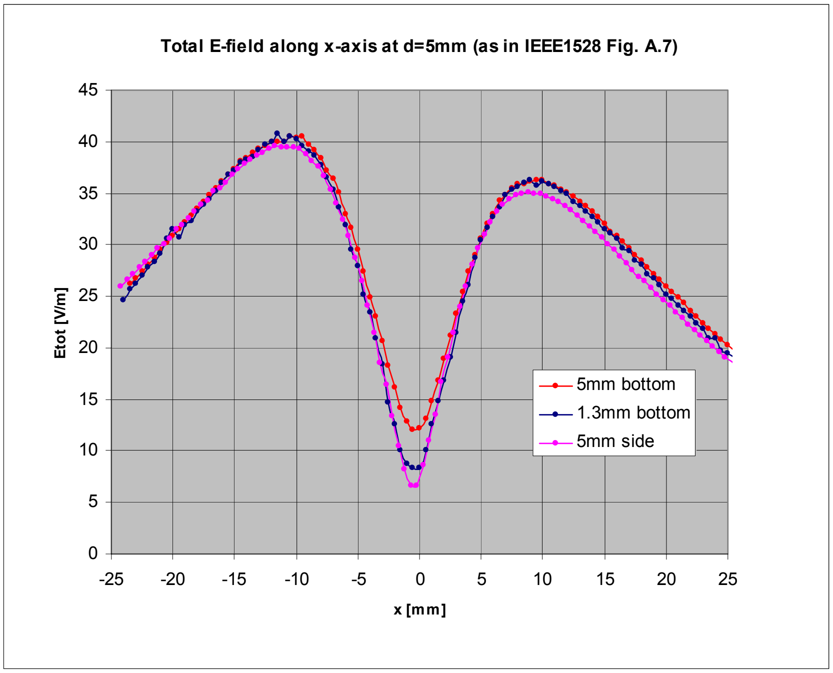

Figure A1.3: Profiles through the dip obtained using measurements every 0.5mm with a 1.3mm probe and with a 5mm probe (see Section A.6 in [1]). For the test done at the side of the box, all the sensors are parallel to the plane of the intended minimum, resulting in better resolution of the minimum and indicating the potential to be realized from sensor offset correction as advanced in this report.

Appendix 2
Outline of steps required of a software algorithm for applying generalized 3D correction algorithm – Virtual Probe Miniaturization (VPM)

1. Make copies of 3D data arrays of raw unlinearized probe output data for each of the three channels.
2. Review each data array prior to processing – zero or negative values may be recorded in the file due to random variability around a notional zero point and these must be addressed. A recommendation is that a zero offset is added to each data point in any array containing values<=0 until the lowest reading is equal to some defined 'floor' of sensitivity. If any of these operations actually need performing on collected data sets, the operations performed need assessing as a percentage error and reporting.
3. Linearise the probe output signals for each channel using appropriate DCPs from the probe calibration data.
4. Evaluate the attenuation constants in each direction for each point of the 3D array.
5. Determine the probe presentation angle and sensor offsets for each measurement point.
6. Compute the correction factors for each point and in each direction.
7. Apply corrections for phantom surface proximity separately for each sensor.
8. Compute the corrected probe outputs for each channel.
9. Apply the probe calibration factors to give results in terms of E or E*E or SAR
10. Report on relevant statistics relating to the VPM conversion to provide assurance that the conversion process has been achieved without introducing anomalies
11. Continue with the remaining post-processing stages.

email: enquiries@indexsar.com http://www.indexsar.com
Oakfield House, Cudworth Lane, Newdigate, Surrey, RH5 5BG, UK.